Compact Integration Rules as a quadrature method with some applications

Víctor J. Llorente[a,*], Antonio Pascau[a]

[a] *Fluid Mechanics Group and LIFTEC, CSIC-University of Zaragoza, María de Luna 3, 50018 Zaragoza, Spain*

Abstract

In many instances of computational science and engineering the value of a definite integral of a known function $f(x)$ is required in an interval. Nowadays there are plenty of methods that provide this quantity with a given accuracy. In one way or another, all of them assume an interpolating function, usually polynomial, that represents the original function either locally or globally. This paper presents a new way of calculating $\int_{x_1}^{x_2} f(x)\,\mathrm{d}x$ by means of compact integration, in a similar way to the compact differentiation employed in computational physics and mathematics. Compact integration is a linear combination of definite integrals associated to an interval and its adjacent ones, written in terms of nodal values of $f(x)$. The coefficients that multiply both the integrals and $f(x)$ at the nodes are obtained by matching terms in a Taylor series expansion. In this implicit method a system of algebraic equations is solved, where the vector of unknowns contains the integrals in each interval of a uniform discrete domain. As a result the definite integral over the whole domain is the sum of all these integrals. In this paper the mathematical tool is analyzed by deriving the appropriate coefficients for a given accuracy, and is exploited in various numerical examples and applications. The great accuracy of the method is highlighted.

Keywords: Numerical integration, Definite integral, Ordinary differential equations, The ENATE scheme.

*Corresponding author

Email addresses: victor.javier.llorente@gmail.com (Víctor J. Llorente), pascau@unizar.es (Antonio Pascau)

1. Introduction

In many branches of science, integral calculus is required in order to calculate any target value of a parameter of the problem under study. For instance, in fluid mechanics, to evaluate the drag or lift coefficient of a solid body it is necessary to perform some integral evaluation on the body surface. After solving the fluid equations, the force $\mathbf{f}$ of interaction between fluid and solid requires a surface integral S of the pressure p and the viscous stress tensor $\mathbf{T}$ in the direction of $\mathbf{n}$, i.e.,

$$\mathbf{f} = -\int_S p\mathbf{n}\,\mathrm{d}S + \int_S \mathbf{T}\mathbf{n}\,\mathrm{d}S.$$

In statistics, the likelihood P that a random variable X falls in a specific range $[a, b]$ will be given by the integral of the probability density function p_X,

$$P\left[a \leq X \leq b\right] = \int_a^b p_X(x)\,\mathrm{d}x,$$

or in solid mechanics, the force lines are calculated with the integrals of the stress field σ_{ij} as

$$y(x) - y_0 = \int_{x_0}^{x} \left(-r(t) \pm \sqrt{1 + r(t)^2}\right) \mathrm{d}t, \quad r = \frac{\sigma_{xx} - \sigma_{yy}}{2\sigma_{xy}}.$$

The previous examples show the ubiquity of integral evaluation. Few analytical solutions of these integrals may be found for practical cases, so one has to resort to numerical integration. The solution accuracy will depend on the nature of the integrand and on the strategy adopted. Let us take for example a one-dimensional integral $\int_{x_1}^{x_2} f(x)\mathrm{d}x$ rearranged as $\Delta x \int_0^1 f(\tilde{x})\mathrm{d}\tilde{x}$ via a mapping to a unity interval, where $\tilde{x} = (x - x_1)/\Delta x$ and $\Delta x = x_2 - x_1$. A wide choice of approximations with different orders of accuracy is available, a relatively short

list is provided below.

$$\begin{aligned}
\int_0^1 f(\tilde{x})\,\mathrm{d}\tilde{x} \approx & \frac{1}{6}\left[f(0)+4f\left(\frac{1}{2}\right)+f(1)\right] \quad \text{Simpson's rule,}\\
\approx & \frac{1}{90}\left[7f(0)+32f\left(\frac{1}{4}\right)+12f\left(\frac{1}{2}\right)+32f\left(\frac{3}{4}\right)+7f(1)\right] \quad \text{Boole's rule,}\\
\approx & \frac{1}{2}\left[f\left(\frac{\sqrt{3}+1}{2\sqrt{3}}\right)+f\left(\frac{\sqrt{3}-1}{2\sqrt{3}}\right)\right] \quad \text{Gauss 2 points,}\\
\approx & \frac{1}{2}\left[\frac{5}{9}f\left(\frac{\sqrt{5}+\sqrt{3}}{2\sqrt{5}}\right)+\frac{8}{9}f\left(\frac{1}{2}\right)+\frac{5}{9}f\left(\frac{\sqrt{5}-\sqrt{3}}{2\sqrt{5}}\right)\right] \quad \text{Gauss 3 points,}\\
\approx & \frac{1}{2}\left[f(0)+f(1)\right]+\frac{1}{12}\left[f'(0)-f'(1)\right] \quad \text{Cubic Hermite,}\\
\approx & \frac{1}{2}\left[f(0)+f(1)\right]+\frac{1}{10}\left[f'(0)-f'(1)\right]+\frac{1}{120}\left[f''(0)+f''(1)\right] \quad \text{Quintic Hermite.}
\end{aligned}$$

If $f(\tilde{x})$ is analytic with no primitive, any of the above formulae would serve. Nevertheless, a different situation occurs when $f(\tilde{x})$ is a sample data. Both quadrature rules, Simpson's and Boole's, as well as Gaussian quadrature rules, require values of $f(\tilde{x})$ at points inside the interval that are not directly available. If the global integral is only what is wanted, the first two quadrature rules can provide the integral value every two points (Simpson's rule) or every four points (Boole's rule) and then summed up for the whole domain. Thus, an even, or multiple of four, number of intervals is mandatory if no interpolation is employed. In the case of Gaussian quadrature an interpolant is needed in order to obtain function values at Gauss points. On the other hand, if Hermite splines are used as interpolants of $f(\tilde{x})$ as in the last two expressions, additional information on derivatives is necessary, that again it is not always available. Thus, every quadrature has its drawbacks. As an alternative to the approaches mentioned, this paper focusses on developing an integration method that only uses the values of the integrand in specific points (nodes), whatever order of accuracy is sought.

Section 2 shows the whole mathematical background and the rules that were obtained for different orders of accuracy with a special treatment at boundary points. In section 3 an analysis of the coefficient matrix that results from the rules derivation is put forward before dealing with the Fourier analysis of er-

rors in section 4, where the dispersion and diffusion errors are estimated. The analogy between the proposed quadrature and multistep methods is described in section 5. The numerical tests in section 6 are divided into four cases. The first three assess the accuracy of compact integration with a sample, an analytic function, and the integral over an infinite domain. The fourth test came up as part of a new method of solving convection diffusion equations named ENATE (**E**nhanced **N**umerical **A**pproximation of a **T**ransport **E**quation) proposed by one of the authors. Finally some conclusions are drawn in section 7.

2. Problem setting - Background

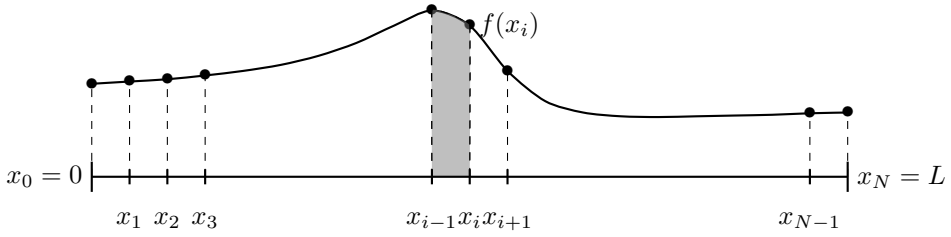

Figure 1: Domain of $f(x)$ splits in N intervals of equal length ($h = L/N$).

We develop a method to calculate the integral of a real function $f(x)$, smooth and continuous over the domain $[0, L]$. The function can be given analytically or as a data set at evenly distributed nodes. The integral in each interval (gray area in Figure 1) is put in terms of a linear combination of adjacent integrals in the left-hand side (LHS), and $f(x_{i+k})$, $k \in \mathbb{Z}$, in the right-hand side (RHS). The number of k's will depend on the order of accuracy sought. The method is named CIR (**C**ompact **I**ntegration **R**ules), and is analogous to the compact differentiation [1].

The generic linear combination of definite integrals centered at (x_{i-1}, x_i) for internal points is given by

$$\sum_{k=-B_1}^{B_2} \alpha_k \int_{x_{i+k-1}}^{x_{i+k}} f(x)\,\mathrm{d}x = h \sum_{k=-S_1}^{S_2} a_k f(x_{i+k}) + TE_i, \tag{1}$$

where $B_{1,2} \in \mathbb{N}_0$ and $S_{1,2} \in \mathbb{N}_0$ are the lower/upper bounds of the stencil for the definite integrals and the function values, respectively. If we define the vector of integrals at every interval as

$$\bar{\mathbf{f}} = \frac{1}{h}\left(\int_{x_0}^{x_1} f(x)\,\mathrm{d}x,\ \int_{x_1}^{x_2} f(x)\,\mathrm{d}x,\ \cdots,\ \int_{x_{N-1}}^{x_N} f(x)\,\mathrm{d}x\right)^T,$$

and the integrand at nodes,

$$\mathbf{f} = (f_0,\ f_1,\ \cdots,\ f_N)^T,$$

the CIR method ends up by solving the linear system

$$\mathbf{M}\bar{\mathbf{f}} \simeq \mathbf{Q}\mathbf{f}, \tag{2}$$

where $\mathbf{M}$ is an N-by-N band-matrix that stores the parameters α_k and $\mathbf{Q}$ is an N-by-$(N+1)$ band-matrix of a_k's. Note that if $B_1 = B_2 = 0$, $\mathbf{M}$ is a diagonal matrix and the quadrature is explicit. The development of CIR will be described in detail for some special cases of equation (1). In particular, symmetry in the LHS will be assumed with $\alpha_0 = 1$. The detailed analysis will be restricted to a matrix of five diagonals in the LHS, $B_1 = B_2 = 2$, and six diagonals in the RHS, $S_1 = 3$ and $S_2 = 2$, that is

$$\begin{aligned}&\beta\int_{x_{i-3}}^{x_{i-2}} f(x)\,\mathrm{d}x + \alpha\int_{x_{i-2}}^{x_{i-1}} f(x)\,\mathrm{d}x + \int_{x_{i-1}}^{x_i} f(x)\,\mathrm{d}x + \alpha\int_{x_i}^{x_{i+1}} f(x)\,\mathrm{d}x + \beta\int_{x_{i+1}}^{x_{i+2}} f(x)\,\mathrm{d}x \\ &= h\left[af(x_{i-3}) + bf(x_{i-2}) + cf(x_{i-1}) + df(x_i) + ef(x_{i+1}) + gf(x_{i+2})\right] + TE_i.\end{aligned} \tag{3}$$

The last term is the error made in the linear combination, it is not the error in the evaluation of the integral $\int_{x_{i-1}}^{x_i} f(x)\,\mathrm{d}x$. Throughout the paper we will characterize each scheme by its local truncation error, TE_i, defined as the leading order of the error in the linear combination. The integrals of every interval have the same order of truncation error as the linear combination. As shown later, the global truncation error of the integral over the whole domain is one order of accuracy less. In the wavenumber analysis and the results section as

we are mainly interested in the errors in the integral of the whole domain, the rules will be named according to the global truncation error.

The system of equations has a coefficient matrix that could be tri- or penta-diagonal depending on whether β is zero or not. On the other hand $\{a, b, c, d, e, g\}$ are linked with $\{\alpha, \beta\}$ when matching the Taylor series coefficients until the desired order of accuracy. The truncation error is related to the first term of the Taylor series that cannot be made zero by the chosen coefficients.

The notation used in the paper for the integral and the integrand is

$$\int_{x_0}^{x_{i+k}} f(x)\,\mathrm{d}x = F_{i+k}, \quad f(x_{i+k}) = f_{i+k}, \quad k \in \mathbb{Z}.$$

In a uniform mesh the Taylor expansion centered at x_i of the above variables is given by

$$f_{i+k} = f_i + khf_i^{(1)} + \frac{k^2h^2}{2!}f_i^{(2)} + \cdots + \frac{k^nh^n}{n!}f_i^{(n)} + \cdots, \tag{4a}$$

$$F_{i+k} = F_i + khf_i + \frac{k^2h^2}{2!}f_i^{(1)} + \frac{k^3h^3}{3!}f_i^{(2)} + \cdots + \frac{k^{n+1}h^{n+1}}{(n+1)!}f_i^{(n)} + \cdots, \tag{4b}$$

where $f_i^{(p)}$ is a p-order (≥ 1) derivative and n a generic term. Equation (4b) is related to a definite integral within $[x_i, x_{i+k}]$ if $k > 0$ or $[x_{i+k}, x_i]$ if $k < 0$. In equation (3), the integration limits go from x_{i+k-1} to x_{i+k}. So, in that case, the integrals of the vector $\overline{\mathbf{f}}$ are computed as $\overline{f}_{i+k} = (F_{i+k} - F_{i+k-1})/h$ in order to cancel out F_i.

2.1. Local third-order family

Let us begin with a simple low order rule where we match the f_i and the $f_i^{(1)}$ terms as shown below.

$$\beta\left(hf_i + \frac{\left(2^2-3^2\right)h^2}{2!}f_i^{(1)}\right) + \alpha\left(hf_i + \frac{\left(1-2^2\right)h^2}{2!}f_i^{(1)}\right) +$$
$$\left(hf_i - \frac{h^2}{2!}f_i^{(1)}\right) + \alpha\left(hf_i + \frac{h^2}{2!}f_i^{(1)}\right) + \beta\left(hf_i + \frac{\left(2^2-1\right)h^2}{2!}f_i^{(1)}\right) \simeq$$
$$h\left[a\left(f_i - 3hf_i^{(1)}\right) + b\left(f_i - 2hf_i^{(1)}\right) + c\left(f_i - hf_i^{(1)}\right) +\right.$$
$$\left. df_i + e\left(f_i + hf_i^{(1)}\right) + g\left(f_i + 2hf_i^{(1)}\right)\right].$$

Taking the first two terms of each expansion, a set of two equations is obtained by equating the factors that multiply f_i and $f_i^{(1)}$ to zero:

$$\begin{aligned} a+b+c+d+e+g =& 1+2\alpha+2\beta, \\ 3^1a+2^1b+c-e-2^1g =& 1!\frac{1+2\left(2^1-1\right)\alpha+\left(1-2^3+3^2\right)\beta}{2!}. \end{aligned}$$

As there are eight coefficients and only two equations to be satisfied there are six arbitrary values. As an example, one can take $a = b = e = g = 0$ then $c = d = (1 + 2\alpha + 2\beta)/2$ where α and β are still arbitrary. The local truncation error is

$$TE_i = -\left(\frac{1-10\alpha-46\beta}{2}\right)\frac{h^3}{3!}f_i^{(2)}.$$

The local order of accuracy is the power of the interval size contained in the local truncation error. In this rule the local truncation error is proportional to h^3 so the order of accuracy is 3.

There is a number of values of $\{\alpha, \beta\}$ that make this term zero, those that satisfy $10\alpha + 46\beta = 1$. In those cases the order of accuracy increases two orders of magnitude,

$$TE_i = -\left(\frac{38\alpha-502\beta-11}{6}\right)\frac{h^5}{5!}f_i^{(4)}.$$

The same increase happens for rules of any odd order of the local truncation error for a certain combination of α and β. Incidentally, if $\alpha = \beta = 0$ the integral is explicit and the Trapezoidal rule over each interval $[x_{i-1}, x_i]$ is recovered, i.e.,

$$\int_{x_{i-1}}^{x_i} f(x)\mathrm{d}x \simeq \frac{h}{2}\left(f_{i-1}+f_i\right).$$

Following this procedure we can obtain the integral in all intervals into which the whole domain has been split. The integral from 0 to L can be calculated by the integration additive property. For instance, by taking the trapezoidal rule for each interval and summing up for the whole domain the composite Trapezoidal rule is obtained,

$$\int_0^L f(x)\mathrm{d}x = \frac{h}{2}\left(f_0+2\sum_{i=1}^{N-1}f_i+f_N\right)-\frac{h^2L}{12}f_\xi^{(2)},$$

where ξ is some point within $[0, L]$. The last term of the expression has been rearranged as an average of values of the second derivative, $f_i^{(2)}$, at each interval $[x_{i-1}, x_i)$,

$$\sum_{i=1}^{N} -\frac{h^3}{12} f_i^{(2)} = -\frac{h^2 hN}{12} \frac{\sum_{i=1}^{N} f_i^{(2)}}{N} = -\frac{h^2 L}{12} f_\xi^{(2)}.$$

The order of accuracy for the integral over the whole domain is 2.

2.2. Local fifth-, seventh- and ninth-order family

Similarly, the set of equations to be satisfied for several orders of accuracy of the local truncation error is presented in this subsection. The coefficients have to satisfy up to equation (6) for 5^{th}-order, up to equation (7) for 7^{th}-order, and up to equation (8) for 9^{th}-order.

$$a + b + c + d + e + g = 1 + 2\alpha + 2\beta, \tag{5}$$

$$\begin{aligned}
3^1 a + 2^1 b + c - e - 2^1 g &= 1! \frac{1 + 2\left(2^1 - 1\right)\alpha + \left(1 - 2^3 + 3^2\right)\beta}{2!}, \\
3^2 a + 2^2 b + c + e + 2^2 g &= 2! \frac{1 + 2^3\alpha + \left(3^3 - 1\right)\beta}{3!}, \\
3^3 a + 2^3 b + c - e - 2^3 g &= 3! \frac{1 + 2\left(2^3 - 1\right)\alpha + \left(1 - 2^5 + 3^4\right)\beta}{4!}, \qquad (6) \\
3^4 a + 2^4 b + c + e + 2^4 g &= 4! \frac{1 + 2^5\alpha + \left(3^5 - 1\right)\beta}{5!}, \\
3^5 a + 2^5 b + c - e - 2^5 g &= 5! \frac{1 + 2\left(2^5 - 1\right)\alpha + \left(1 - 2^7 + 3^6\right)\beta}{6!}, \qquad (7) \\
3^6 a + 2^6 b + c + e + 2^6 g &= 6! \frac{1 + 2^7\alpha + \left(3^7 - 1\right)\beta}{7!}, \\
3^7 a + 2^7 b + c - e - 2^7 g &= 7! \frac{1 + 2\left(2^7 - 1\right)\alpha + \left(1 - 2^9 + 3^8\right)\beta}{8!}. \qquad (8)
\end{aligned}$$

A family rule which has a fifth-order local TE_i can be given by the following set of coefficients:

$$a = g = 0, \qquad b = e = \frac{10\alpha + 46\beta - 1}{24}, \qquad c = d = \frac{14\alpha - 22\beta + 13}{24}.$$

It should be mentioned that the same values of α and β that made the third-order local truncation error vanish, also cause the pair $\{b, e\}$ to become zero in

the fifth-order family. As seen before, this particular pair of values of $\{\alpha, \beta\}$ leads the rule to fifth-order accuracy. In the same way, when taking $\beta = 0$ and $\alpha = 1/10$, a fifth-order rule with a two-point stencil in the RHS is obtained,

$$\frac{1}{10}\int_{x_{i-2}}^{x_{i-1}} f(x)\mathrm{d}x + \int_{x_{i-1}}^{x_i} f(x)\mathrm{d}x + \frac{1}{10}\int_{x_i}^{x_{i+1}} f(x)\mathrm{d}x \simeq \frac{3h}{5}\left[f_{i-1} + f_i\right]. \quad (9)$$

When $\alpha = 11/38$ the fifth-order local truncation error goes to zero and a seventh-order accuracy is attained with a four-point stencil in the RHS by

$$\begin{aligned}&\frac{11}{38}\int_{x_{i-2}}^{x_{i-1}} f(x)\mathrm{d}x + \int_{x_{i-1}}^{x_i} f(x)\mathrm{d}x + \frac{11}{38}\int_{x_i}^{x_{i+1}} f(x)\mathrm{d}x \\ &\simeq \frac{h}{38}\left[3f_{i-2} + 27f_{i-1} + 27f_i + 3f_{i+1}\right]. \end{aligned} \quad (10)$$

Leaving α and β as free parameters, the seventh-order family becomes

$$\begin{aligned} a = g = -\frac{38\alpha - 502\beta - 11}{1440}, \qquad b = e = \frac{238\alpha + 418\beta - 31}{480}, \\ c = d = \frac{382\alpha - 158\beta + 401}{720}. \end{aligned}$$

Finally, solving the whole system of equations, a ninth-order family with only one free parameter β is obtained as follows:

$$\begin{aligned} a = g = \frac{3\left(478\beta - 3\right)}{5420}, \qquad b = e = \frac{3\left(4426\beta + 199\right)}{5420}, \\ c = d = \frac{24\left(83\beta + 42\right)}{1355}, \qquad \alpha = \frac{1726\beta + 191}{542}. \end{aligned}$$

Taking $\beta = 0$ a ninth-order scheme with a six-point stencil in the RHS can be obtained,

$$\begin{aligned}&\frac{191}{542}\int_{x_{i-2}}^{x_{i-1}} f(x)\mathrm{d}x + \int_{x_{i-1}}^{x_i} f(x)\mathrm{d}x + \frac{191}{542}\int_{x_i}^{x_{i+1}} f(x)\mathrm{d}x \simeq \\ &\frac{h}{5420}\left[-9f_{i-3} + 597f_{i-2} + 4032f_{i-1} + 4032f_i + 597f_{i+1} - 9f_{i+2}\right]. \end{aligned} \quad (11)$$

For the $(n+1)$th-order families the local truncation error can be written as

$$\begin{aligned} TE_i = &\Big[1 + 2^{n+1}\alpha + \left(3^{n+1} - 1\right)\beta - \\ &\left(n+1\right)\left(3^n a + 2^n b + c + e + 2^n g\right)\Big]\frac{h^{n+1}}{(n+1)!}f_i^{(n)}, \end{aligned} \quad (12)$$

and listed in Table 1 for different values of weights and parameters.

Ninth order can be achieved with a RHS stencil of six points. If greater accuracy is sought one can increase the stencil, the number of neighbour integrals considered or both, to let more Taylor coefficients match in the left- and right-hand sides of equation (1). Furthermore, the study of family rules need not be limited to odd orders. For instance, to derive a local fourth-order family the system of equations is

$$\begin{aligned} a+b+c+d+e+g &= 1+2\alpha+2\beta, \\ 3^1a+2^1b+c-e-2^1g &= 1!\frac{1+2\left(2^1-1\right)\alpha+\left(1-2^3+3^2\right)\beta}{2!}, \\ 3^2a+2^2b+c+e+2^2g &= 2!\frac{1+2^3\alpha+\left(3^3-1\right)\beta}{3!}. \end{aligned}$$

Taking $\beta = 0$ and $a = e = g = 0$, the family rule with free α becomes

$$b = \frac{10\alpha-1}{12}, \quad c = \frac{2(1-\alpha)}{3}, \quad d = \frac{22\alpha+5}{12},$$

with the truncation error being

$$TE_i = (1-10\alpha)\frac{h^4}{4!}f_i^{(3)}.$$

If $\alpha = 1/10$ the rule (9) is recovered.

2.3. CIR at Boundaries

The whole background for internal points has been provided, but it is necessary, in closing the algebraic system, to treat the integrals of $f(x)$ at both boundaries using the same strategy of matching Taylor series terms. A general boundary rule centered at (x_{p-1}, x_p) close to x_0 could be

$$\sum_{k=-B_{c1}}^{B_{c2}} \alpha_k \int_{x_{p+k-1}}^{x_{p+k}} f(x)\,\mathrm{d}x = h\sum_{k=0}^{S_c} a_k f(x_k) + TE_p,$$

where B_{c2}, $S_c \in \mathbb{N}_0$ and $\{B_{c1} \in \mathbb{N}_0 |\, 0 \le B_{c1} \le p-1\}$. The equivalent rule close to x_N reads

$$\sum_{k=-B_{c1}}^{B_{c2}} \alpha_k \int_{x_{p-k-1}}^{x_{p-k}} f(x)\,\mathrm{d}x = h\sum_{k=0}^{S_c} a_k f(x_{N-k}) + TE_p,$$

a, g	b, e	c, d	α	β	TE_i
		$\frac{1}{2}$			$-\frac{h^3}{12} f_i^{(2)}$
		$\frac{1+2\alpha+2\beta}{2}$	α	β	$-\left(\frac{1-10\alpha-46\beta}{2}\right) \frac{h^3}{3!} f_i^{(2)}$
	$\frac{10\alpha+46\beta-1}{24}$	$\frac{14\alpha-22\beta+13}{24}$	α	β	$-\left(\frac{38\alpha-502\beta-11}{6}\right) \frac{h^5}{5!} f_i^{(4)}$
		$\frac{3}{5}$	$\frac{1}{10}$		$-\frac{h^5}{100} f_i^{(4)}$
$-\frac{38\alpha-502\beta-11}{1440}$	$\frac{238\alpha+418\beta-31}{480}$	$\frac{382\alpha-158\beta+401}{720}$	α	β	$-\left(\frac{191-542\alpha+1726\beta}{12}\right) \frac{h^7}{7!} f_i^{(6)}$
	$\frac{3}{38}$	$\frac{27}{38}$	$\frac{11}{38}$		$-\frac{3h^7}{5320} f_i^{(6)}$
$\frac{3(478\beta-3)}{5420}$	$\frac{3(4426\beta+199)}{5420}$	$\frac{24(83\beta+42)}{1355}$	$\frac{1726\beta+191}{542}$	β	$-\frac{216(3762\beta-137)}{1355} \frac{h^9}{9!} f_i^{(8)}$
$-\frac{9}{5420}$	$\frac{597}{5420}$	$\frac{1008}{1355}$	$\frac{191}{542}$		$-\frac{29592}{1355} \frac{h^9}{9!} f_i^{(8)}$

Table 1: Summary of parameters, weights and local truncation errors for eqn.(3). No entry value means that the parameter is equal to zero.

where $\{B_{c1} \in \mathbb{N}_0 | \, 0 \leq B_{c1} \leq N-p\}$. Note that α's and a's are the same for both rules and might be identical or not to the internal ones. The set $\{a_k\}$ links with $\{\alpha_k\}$ via similar expansion (4) centered at x_p. With similar particularizations as before, boundary CIRs at x_0, $p=1$, and x_N, $p=N$, have the form

$$\int_{x_0}^{x_1} f(x)\mathrm{d}x + \alpha \int_{x_1}^{x_2} f(x)\mathrm{d}x =$$
$$h\left[af_0 + bf_1 + cf_2 + df_3 + ef_4 + gf_5 + kf_6\right] + TE_1,$$
$$\alpha \int_{x_{N-2}}^{x_{N-1}} f(x)\mathrm{d}x + \int_{x_{N-1}}^{x_N} f(x)\mathrm{d}x =$$
$$h\left[af_N + bf_{N-1} + cf_{N-2} + df_{N-3} + ef_{N-4} + gf_{N-5} + kf_{N-6}\right] + TE_N,$$

where the local truncation error is

$$TE_{1,N} = \Big[1 + \left(2^{n+1} - 1\right)\alpha - (n+1)\left(b + 2^n c + 3^n d + 4^n e + 5^n g + 6^n k\right)\Big] \frac{h^{n+1}}{(n+1)!} f_{1,N}^{(n)}.$$

For the 9^{th}-order rule and any other with a large stencil in the RHS, an additional boundary expression should be added at x_1 and x_{N-1} since some points of the stencil in (11) are outside the domain. For instance, close to the left

boundary the integral $\int_{x_1}^{x_2} f(x)\mathrm{d}x$ would require $f(x_{-1})$. For this case we have

$$\begin{aligned}
&\alpha_{-1}\int_{x_0}^{x_1} f(x)\mathrm{d}x + \int_{x_1}^{x_2} f(x)\mathrm{d}x + \alpha_1\int_{x_2}^{x_3} f(x)\mathrm{d}x = \\
&h\left[af_0 + bf_1 + cf_2 + df_3 + ef_4 + gf_5\right] + TE_2, \\
&\alpha_1\int_{x_{N-3}}^{x_{N-2}} f(x)\mathrm{d}x + \int_{x_{N-2}}^{x_{N-1}} f(x)\mathrm{d}x + \alpha_{-1}\int_{x_{N-1}}^{x_N} f(x)\mathrm{d}x = \\
&h\left[af_N + bf_{N-1} + cf_{N-2} + df_{N-3} + ef_{N-4} + gf_{N-5}\right] + TE_{N-1},
\end{aligned}$$

with the truncation error being

$$\begin{aligned}
TE_{2,N-1} = &\Big[1 + \left(2^9 - 1\right)\alpha_{-1} + \alpha_1 - \\
&9\left(2^8 a + b + d + 2^8 e + 3^8 g\right)\Big]\frac{h^9}{9!} f^{(8)}_{2,N-1}.
\end{aligned}$$

All parameters and weights are provided in Table 2 and 3 for boundary points. As a remark, a 5^{th}-order boundary rule yields Simpson's rule for the integral between x_0 and x_2. Some of the rules are also provided in Table 2 with a free α but adding this new degree of freedom enlarges the stencil of the RHS by one node. Notice that the ninth-order rule for nodes adjacent to boundary has broken the symmetry to get a shorter stencil in the RHS.

Local order	α	a	b	c	d	e	g	k
3	α	$\frac{1-\alpha}{2}$	$\frac{1+3\alpha}{2}$					
		$\frac{1}{2}$	$\frac{1}{2}$					
5	α	$\frac{9-\alpha}{24}$	$\frac{13\alpha+19}{24}$	$\frac{13\alpha-5}{24}$	$\frac{1-\alpha}{24}$			
	1	$\frac{1}{3}$	$\frac{4}{3}$	$\frac{1}{3}$				
7	α	$\frac{475-27\alpha}{1440}$	$\frac{637\alpha+1427}{1440}$	$\frac{7(73\alpha-57)}{720}$	$\frac{241-129\alpha}{720}$	$\frac{77\alpha-173}{1440}$	$\frac{27-11\alpha}{1440}$	
	$\frac{27}{11}$	$\frac{281}{990}$	$\frac{1028}{495}$	$\frac{196}{165}$	$-\frac{52}{495}$	$\frac{1}{90}$		
9	$-\frac{1375}{56097}$	$\frac{71036879}{212046660}$	$\frac{5684564}{5890185}$	$-\frac{13273643}{23560740}$	$\frac{19246592}{53011665}$	$-\frac{3823643}{23560740}$	$\frac{253964}{5890185}$	$-\frac{1085521}{212046660}$

Table 2: Parameter and weights for boundary rule at x_0 and x_N. No entry value means that the parameter is equal to zero.

α_{-1}	α_1	a	b	c	d	e	g
$\frac{5}{32}$	$\frac{4357}{6112}$	$\frac{2337}{61120}$	$\frac{33687}{61120}$	$\frac{3897}{3820}$	$\frac{258}{955}$	$-\frac{693}{61120}$	$\frac{9}{12224}$

Table 3: Parameter and weights for 9^{th}-order boundary rule at x_1 and x_{N-1}.

2.4. Global truncation error

The global truncation error can be estimated as the sum of all the elements of the vector that results from $\mathbf{M}^{-1}\mathbf{TE}$, that is,

$$TE = \mathbf{1}^T\mathbf{M}^{-1}\mathbf{TE},$$

being $\mathbf{1} = (1, 1, \cdots, 1)^T$. The vector of local truncation errors at each point of the mesh $\{x_i\}$ is written as

$$\mathbf{TE} = h^{n+1}\mathrm{diag}(\boldsymbol{\lambda})\mathbf{f^{(n)}},$$

where $\boldsymbol{\lambda} = (\lambda_1, \lambda_2, \cdots, \lambda_N)^T$ is the vector of constants, that are equal for inner points, and $\mathbf{f^{(n)}} = (f_1^{(n)}, f_2^{(n)}, \cdots, f_N^{(n)})^T$ is the vector of nth-derivative values. So

$$TE = h^{n+1}\boldsymbol{\lambda^\star}\cdot\mathbf{f^{(n)}} \quad \text{with} \quad \boldsymbol{\lambda^\star} = \mathbf{1}^T\mathbf{M}^{-1}\mathrm{diag}(\boldsymbol{\lambda}).$$

It can be rearranged as a weighted average of values for the nth derivative at x_i,

$$TE = h^n hN\,\frac{\boldsymbol{\lambda^\star}\cdot\mathbf{1}}{N}\,\frac{\boldsymbol{\lambda^\star}\cdot\mathbf{f^{(n)}}}{\boldsymbol{\lambda^\star}\cdot\mathbf{1}} = h^n L\,\overline{\lambda^\star}\,f_\xi^{(n)},$$

the truncation error for the integral of the whole domain is $\mathcal{O}\left(h^n\right)$ whereas for the integrals of the intervals is $\mathcal{O}\left(h^{n+1}\right)$.

3. Matrix analysis

The metric of $\mathbf{M}$ is essential to the stability of the numerical solution $\widehat{\overline{\mathbf{f}}}$ of the system (2) via a direct or iterative method. The norm of its inverse can give an estimation of the error in terms of the remainder, $\mathbf{r} = \mathbf{b} - \mathbf{M}\widehat{\overline{\mathbf{f}}}$,

$$||\widehat{\overline{\mathbf{f}}} - \overline{\mathbf{f}}|| \leq ||\mathbf{M}^{-1}||\,||\mathbf{r}||,$$

where $\mathbf{b} = \mathbf{Q}\mathbf{f}$ and $||\cdot||$ any norm. Also, in this section a study on the condition number of the matrix $\mathbf{M}$ is conducted. The condition number, $\kappa(\mathbf{M}) \geq 1$, is related to the response of the system to small perturbations and hence, to the accumulation of round-off errors. With small perturbations the system to solve is $(\mathbf{M} + \delta\mathbf{M})(\bar{\mathbf{f}} + \delta\bar{\mathbf{f}}) \simeq \mathbf{b} + \delta\mathbf{b}$. The change in the solution reads

$$\frac{||\delta\bar{\mathbf{f}}||}{||\bar{\mathbf{f}}||} \leq \frac{\kappa(\mathbf{M})}{1 - \kappa(\mathbf{M})\frac{||\delta\mathbf{M}||}{||\mathbf{M}||}} \left(\frac{||\delta\mathbf{b}||}{||\mathbf{b}||} + \frac{||\delta\mathbf{M}||}{||\mathbf{M}||} \right),$$

being $\kappa(\mathbf{M}) = ||\mathbf{M}||\,||\mathbf{M}^{-1}||$ the condition number. Let us consider a tridiagonal matrix in the form of

$$\mathbf{M} = \begin{pmatrix} 1 & \alpha_B & & & & & & \\ \alpha_{-1,nB} & 1 & \alpha_{1,nB} & & & & & \\ & \alpha_I & 1 & \alpha_I & & & & \\ & & \ddots & \ddots & \ddots & & & \\ & & & \alpha_I & 1 & \alpha_I & & \\ & & & & \alpha_{1,nB} & 1 & \alpha_{-1,nB} \\ & & & & & \alpha_B & 1 \end{pmatrix}.$$

Subscripts I, nB and B stand for internal, near to the boundary and boundary, respectively. The second and the $(N-1)$th row are applied if the points in the RHS exceed the domain limits. In other case, $\alpha_{-1,nB} = \alpha_{1,nB} = \alpha_I$. The maximum of the off-diagonal summation by rows is denoted by

$$\Sigma_{\mathrm{r}} = \max\Big\{|\alpha_B|, |\alpha_{-1,nB}| + |\alpha_{1,nB}|, 2|\alpha_I|\Big\},$$

and by columns,

$$\Sigma_{\mathrm{c}} = \max\Big\{|\alpha_{-1,nB}|, |\alpha_I| + |\alpha_B|, |\alpha_I| + |\alpha_{1,nB}|, 2|\alpha_I|\Big\},$$

and the maximum of the two,

$$\Sigma = \max\left\{\Sigma_{\mathrm{r}}, \Sigma_{\mathrm{c}}\right\}.$$

If $\mathbf{M}$ is strictly diagonal dominant (SDD) by rows, the Ahlberg-Nilson bound [2] yields

$$||\mathbf{M}^{-1}||_{\infty} \leq \frac{1}{1-\Sigma_{\mathrm{r}}}.$$

This result could provide an evaluation of $\kappa_{\infty}(\mathbf{M})$. However, the condition number is more restrictive if it is calculated with the spectral norm. Using *Theorem 2* in Qi [3], an upper bound for the 2-norm condition number is

$$\kappa_2(\mathbf{M}) \leq \frac{1+\Sigma}{1-\Sigma},$$

if $\mathbf{M}$ is SDD by rows and columns.

In table 4 values of $||\mathbf{M}^{-1}||_{\infty}$ and $\kappa_2(\mathbf{M})$ are shown for some matrices employed in CIR and calculated in Matlab. In the last column the estimated upper bounds are also written for those matrices that have one estimate, that is, they are SDD by columns, rows or both. The third matrix in the local fifth-order rule of CIR, the fifth matrix is that of local seventh-order CIR and the last one is that associated to the local ninth-order CIR. The second and fourth matrices are related to rules with α free at boundaries.

The determinant of the first matrix approaches zero as the size tends to infinity. For $N = 5$, $det(\mathbf{M}) = 0.1875$ and for $N = 1000$, $det(\mathbf{M}) = 9.34 \cdot 10^{-299}$. This matrix was used just to check the ability of Matlab to calculate very large condition numbers. The rest of matrices are well-conditioned or weakly ill-conditioned, such as the fifth matrix, where $\kappa_2(\mathbf{M})$ is slightly high but shows an upper bound. The sixth matrix does not have a bound estimate for $\kappa_2(\mathbf{M})$ because is not SDD by columns.

Based on this analysis it can be concluded that all matrices employed in CIR are well-conditioned. The residual of the matrix equation can provide a good estimation of the solution error as the norm of $\mathbf{M}^{-1}$ is of order 1.

α_I	$\alpha_{-1,nB}$	$\alpha_{1,nB}$	α_B	N				Bound estimates
				5	20	100	1000	
$\frac{1}{2}$	$\frac{1}{2}$	$\frac{1}{2}$	$\frac{1}{2}$	9.0000	110.0000	$2.5500 \cdot 10^3$	$2.5050 \cdot 10^5$	
				13.9282	178.0643	$4.1336 \cdot 10^3$	$4.0610 \cdot 10^5$	
$\frac{1}{10}$	$\frac{1}{10}$	$\frac{1}{10}$	$\frac{1}{10}$	1.2470	1.25	1.25	1.25	1.25
				1.4190	1.4930	1.4997	1.5000	1.5
$\frac{1}{10}$	$\frac{1}{10}$	$\frac{1}{10}$	1	2.3636	2.3624	2.3624	2.3624	
				3.1565	3.0873	3.0873	3.0873	
$\frac{1}{10}$	$\frac{11}{38}$	$\frac{11}{38}$	$\frac{1}{10}$	1.7291	1.7145	1.7145	1.7145	2.375
				1.9978	1.7939	1.7939	1.7939	3.75
$\frac{11}{38}$	$\frac{11}{38}$	$\frac{11}{38}$	$\frac{27}{11}$	32.7975	22.8832	22.8832	22.8832	
				71.9585	43.4467	43.4467	43.4467	
$\frac{191}{542}$	$\frac{5}{32}$	$\frac{4357}{6112}$	$-\frac{1375}{56097}$	3.5805	3.4187	3.4001	3.3999	7.64
				6.4116	5.8772	5.8392	5.8388	

Table 4: Infinity norm (top number) and 2-norm condition number (bottom number) for different N-by-N matrices with the upper bounds.

4. Wavenumber analysis

When one works with numerical approximations of differential or integral equations some differences with the exact values are expected due to truncation and round-off errors. If the discrete equations are rewritten by substituting the point values using Taylor series expansion, the original differential/integral equation is obtained with additional terms. These terms cause a numerical dispersion and dissipation in the solution [4, 5, 6, 7]. The use of Fourier analysis for assessing the numerical dispersion and dissipation of schemes, also named as the modified wavenumber approach, is widespread [8, 9, 10, 11]. The numerical behaviour of CIR will be explored next by carrying out a modified wavenumber study.

First, the integrand may be decomposed into a Fourier series as

$$f(x) = \sum_k \hat{f}_k \exp\left(i\omega \frac{x}{h}\right),$$

where $\hat{f}_k$ are the Fourier coefficients, $\omega\,(=2\pi k/N)$ the wavenumber and $i \equiv \sqrt{-1}$. Now, the Fourier series for the exact integral is given by

$$F(x) = \sum_k \widehat{F}_k \exp\left(i\omega\frac{x}{h}\right) \quad \text{with} \quad \widehat{F}_k = -\frac{h\,i}{\omega}\hat{f}_k.$$

However, the Fourier coefficients of the integrals using the rules above,

$$\widehat{F}_k\Big|_{\text{CIR}} = -\frac{h\,i}{\omega_m(\omega)}\hat{f}_k,$$

might not be the same as $\widehat{F}_k$. ω_m is the numerical wavenumber. An exact integration would give $\omega_m = \omega$, thus the difference between both is an indication of the quality of the method. Therefore, replacing

$$f(x+ph) = \sum_k \hat{f}_k \exp\left(p\,i\omega\right) \exp\left(i\omega\frac{x}{h}\right), \quad p \in \{-3,-2,-1,1,2\},$$

in the RHS of equation (3), and

$$F(x+ph)|_{\text{CIR}} = \sum_k -\frac{h\,i}{\omega_m}\hat{f}_k \exp\left(p\,i\omega\right) \exp\left(i\omega\frac{x}{h}\right), \quad p \in \{-3,-2,-1,1,2\},$$

in the LHS, using Euler's formula and some algebra, the real $\Re(\omega_m)$ and imaginary $\Im(\omega_m)$ parts read

$$\Re(\omega_m) = \frac{r_1 s_1 + r_2 s_2}{s_1^2 + s_2^2}, \quad \Im(\omega_m) = \frac{r_2 s_1 - r_1 s_2}{s_1^2 + s_2^2}, \tag{13}$$

where

$$\begin{aligned}
r_1 &= (1+\beta)\sin(\omega) + \alpha\sin(2\omega) + \beta\sin(3\omega)\,,\\
r_2 &= (\alpha-1) + (1-2\alpha+\beta)\cos(\omega) + (\alpha-2\beta)\cos(2\omega) + \beta\cos(3\omega)\,,\\
s_1 &= d + (e+c)\cos(\omega) + (g+b)\cos(2\omega) + a\cos(3\omega)\,,\\
s_2 &= (e-c)\sin(\omega) + (g-b)\sin(2\omega) - a\sin(3\omega)\,.
\end{aligned}$$

As quoted in Lele [1], the real part of the numerical wavenumber is associated with the dispersive error and the imaginary part with dissipative errors. For boundary rules at x_0 and x_N, the Fourier steps are the same and the coefficients of equation (13) are

$$
\begin{aligned}
r_1 &= (1-\alpha)\sin(\omega) + \alpha\sin(2\omega)\,,\\
r_2 &= 1-(1-\alpha)\cos(\omega) - \alpha\cos(2\omega)\,,\\
s_1 &= a + b\cos(\omega) + c\cos(2\omega) + d\cos(3\omega) + e\cos(4\omega) + g\cos(5\omega) + k\cos(6\omega)\,,\\
s_2 &= b\sin(\omega) + c\sin(2\omega) + d\sin(3\omega) + e\sin(4\omega) + g\sin(5\omega) + k\sin(6\omega)\,.
\end{aligned}
$$

The boundary rule at x_1 and x_{N-1} has $k = 0$ in s_1 and s_2, and r_1 and r_2 become

$$
\begin{aligned}
r_1 &= (\alpha_1 - 1)\sin(\omega) + (1-\alpha_2)\sin(2\omega) + \alpha_2\sin(3\omega)\,,\\
r_2 &= \alpha_1 - (1-\alpha_1)\cos(\omega) + (\alpha_2 - 1)\cos(2\omega) - \alpha_2\cos(3\omega)\,.
\end{aligned}
$$

In all figures the rules are named according to their global truncation error. In Figure 2, there are several rules for which the modified wavenumber for inner points skyrockets before dropping very quickly to be zero at π (drop not shown). It is also seen that (e)-(g)-(h) are relatively good approximations within a reasonable range of ω. As the order of these tridiagonal rule rises, it is moving closer to the exact ω for low-middle wavenumber values.

To quantify whether a numerical scheme is well-resolvable, the modified wavenumber must approximate the exact wavenumber within an appropriate error tolerance,

$$
\frac{|\Re(\omega_m) - \omega|}{\omega} \leq \varepsilon. \tag{14}
$$

The interval $[0, \omega_r]$ where the above condition is met is the acceptable range of approximation and, therefore, the fraction $\eta(\varepsilon) = \omega_r/\pi$ is the resolving efficiency of a scheme that shows how poorly or well the waves are being resolved. Given

the schemes in figure 2, the efficiency is determined for different tolerance values $\{0.1, 0.01, 0.001\}$ and tabulated in Table 5.

Scheme	$\varepsilon = 0.1$	$\varepsilon = 0.01$	$\varepsilon = 0.001$	Global order
(b)	0.329	0.109	0.034	2nd
(c)	0.25	0.078	0.024	
(e)	0.557	0.327	0.186	4th
(g)	0.706	0.516	0.365	6th
(h)	0.762	0.602	0.465	8th

Table 5: Resolving efficiency for different inner schemes plotted in figure 2.

Overall, these results indicate that the scheme (h) stays close to the exact integration (a) in almost half of the wavenumber spectrum for extremely small tolerances. In the cases of scheme (e) and (g), waves are being resolved properly for small and moderate tolerances. On the other hand, the scheme (d) never meets condition (14) nor scheme (f), so their efficiencies are zero for the values of ε in Table 5. Both schemes are pentadiagonal and achieved a poor resolution. However, this does not suggest that some other pentadiagonal family would score as bad. Within a family with the same LHS stencil the efficiency depends on the particular scheme.

Additionally, in Figure 3 the numerical imaginary wavenumber is zero in all rules except (d) and (f). The numerator of the imaginary part of equation (13) is given in Table 6. It may be seen that in a global second-order family with $\beta = 0$ or $\beta = -(1 + 2\alpha)/2$, $\Im(\omega_m)$ goes to zero. For the case of a global fourth-order family, $\Im(\omega_m)$ vanishes when $\beta = 0$ or $\alpha = -2/3$ and $\beta = 1/6$; and only for $\beta = 0$ in a global sixth-, eighth-order family. Pentadiagonal sixth- and eighth-orders are not shown since they behave like (f) or worse.

On the other hand, in Figures 4 and 5 for boundaries, almost all rules tend to be close to the exact integration for the low-middle ω region. However, huge differences turn up in the boundary of the global eighth-order rule (e) and (f). Including the additional information of the integral near the boundary

Family global order	$\Im(\omega_m)$-num.
2th	$\beta \sin^2(\omega)\left[1+2(\alpha+\beta)\right]$
4th	$\beta \sin^2(\omega)\left[\frac{10\alpha+46\beta-1}{6}\cos(\omega)+\frac{2\alpha-34\beta+7}{6}\right]$
6th	$-\beta \sin^2(\omega)\left[\frac{38\alpha-502\beta-11}{188}\cos^2(\omega)-\frac{376\alpha+376\beta-52}{188}\cos(\omega)-\frac{22\alpha-518\beta+221}{188}\right]$
8th	$6\,\beta \sin^2(\omega)\left[\frac{478\beta-3}{1355}\cos^2(\omega)+\frac{1974\beta+101}{1355}\cos(\omega)+\frac{287-562\beta}{1355}\right]$

Table 6: Numerator of the numerical wavenumber (imaginary).

and/or shortening the stencil by breaking the symmetry in the LHS, changes considerably the accuracy of the rule.

In turn, the resolvable efficiency for boundaries has been computed in table 7. The efficiencies of almost all schemes at boundaries are very close to those at internal points of the same order, independently of the error tolerance. Nonetheless the scheme (g) has low efficiencies in contrast to its inner scheme of the same order (h). Similarly, the scheme (f) breaks the trend for high tolerance values within the 6th-order family rules.

Scheme	$\varepsilon = 0.1$	$\varepsilon = 0.01$	$\varepsilon = 0.001$	Global order
(b)	0.329	0.109	0.034	2nd
(c)	0.593	0.355	0.204	4th
(d)	0.581	0.273	0.148	
(e)	0.715	0.483	0.325	6th
(f)	0.508	0.396	0.349	
(g)	0.513	0.371	0.243	8th
(h)	0.777	0.603	0.460	

Table 7: Resolving efficiency for different boundary schemes plotted in figure 4.

5. CIR as linear multistep method

In this section an analogy between CIR and linear multistep methods for ODE is established. It will be theoretically shown that if CIR is cast as a linear

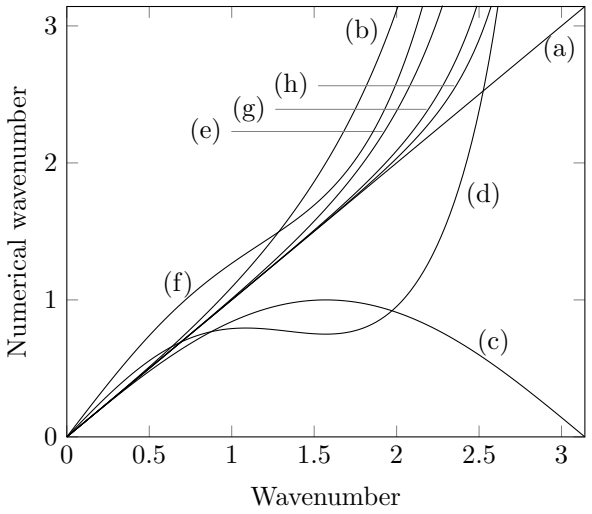

Figure 2: Numerical wavenumber vs wavenumber for inner points: (a) Exact Integration; (b) Trapezoidal rule, (c) Tridiagonal second order ($\alpha = 1/2$); (d) Pentadiagonal second order ($\alpha = \beta = 1/2$); (e) Tridiagonal fourth order ($\alpha = 1/10$); (f) Pentadiagonal fourth order ($\alpha = \beta = 1/10$); (g) Tridiagonal sixth order ($\alpha = 11/38$); (h) Tridiagonal eighth order ($\alpha = 191/542$).

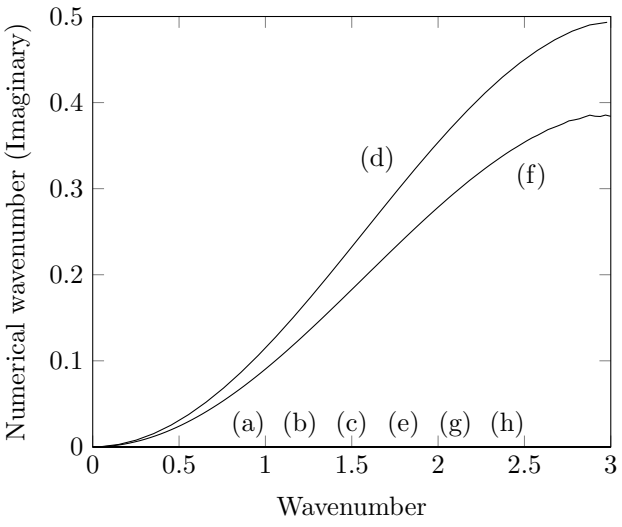

Figure 3: Numerical wavenumber (Imaginary) vs wavenumber for inner points: same notation as Figure 2.

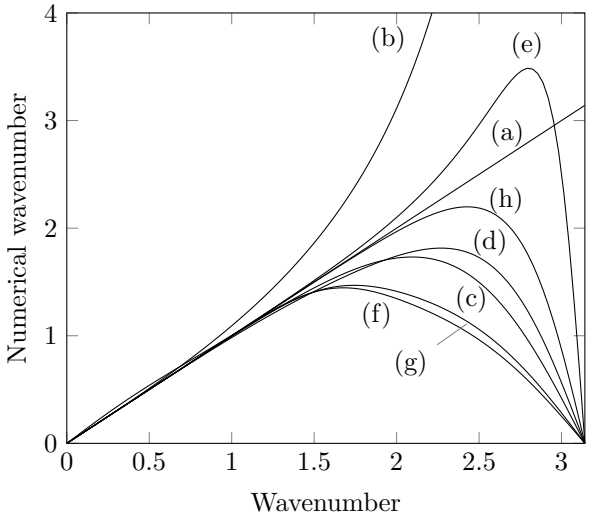

Figure 4: Numerical wavenumber vs wavenumber of boundaries: (a) Exact Integration, (b) Second order ($\alpha = 0$), (c) Fourth order ($\alpha = 1$ or Simpson's rule), (d) Fourth order ($\alpha = 1/10$), (e) Sixth order ($\alpha = 27/11$), (f) Sixth order ($\alpha = 11/38$), (g) Eighth order at $x_0|x_N$, (h) Eighth order at $x_1|x_{N-1}$.

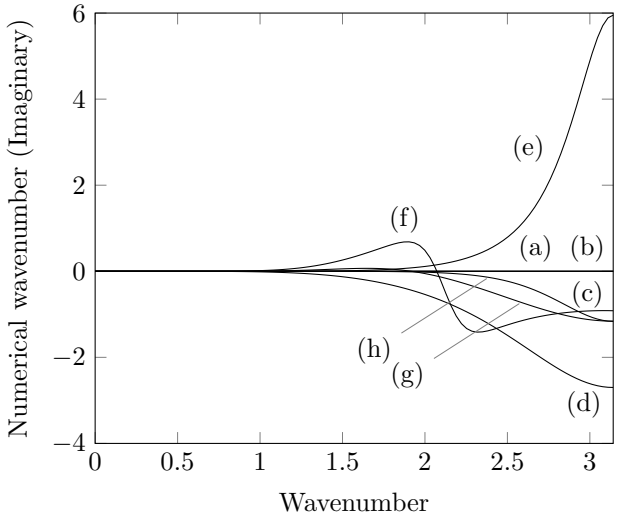

Figure 5: Numerical wavenumber (Imaginary) vs wavenumber of boundaries: same notation as Figure 4.

multistep method it is not stable but when used as originally proposed, that is, a system of equations, it can provide very accurate solutions without stability problems in the iterative matrix solver, at least for the numerical tests proposed. CIR can compute the 1D integral

$$F(x) = \int_{x_0}^{x} f(t)\,\mathrm{d}t,$$

being t the integration variable. In a general case, the integrand f may depend on F, thus dealing with an integral equation

$$F(x) = \int_{x_0}^{x} f(t, F(t))\,\mathrm{d}t.$$

As will be shown CIR can also be interpreted as a linear multistep method applied to the first-order ODE

$$F'(x) = f(x, F(x)), \quad F(x_0) = 0.$$

In a linear multistep method F' is approximated as a linear combination of the discrete integrals $\{F_i\}$ at equally spaced mesh points $\{x_i\}$ and the RHS is computed by a linear combination of f values at the same points.

$$\sum_{s=0}^{m} \lambda_s F_{i+s} = h \sum_{s=0}^{m} \mu_s f_{i+s}.$$

Coefficients λ_s and μ_s are determined by Taylor expansion matching, numerical integration, or interpolation. If the integrals in equation (3) are separated as

$$\int_{x_{i+k-1}}^{x_{i+k}} f(x)\,\mathrm{d}x = F_{i+k} - F_{i+k-1}, \quad k \in \{0, \pm 1, \pm 2\},$$

and the F-terms are grouped with a previous shift of indices, e.g. $F_{i-3} \to F_i$ and so on, then the recurrence relation reads

$$\begin{aligned} &\beta F_{i+5} + (\alpha - \beta)\, F_{i+4} + (1-\alpha) F_{i+3} - (1-\alpha) F_{i+2} - \\ &(\alpha - \beta) F_{i+1} - \beta F_i = h\Big[g f_{i+5} + e f_{i+4} + d f_{i+3} + \\ &c f_{i+2} + b f_{i+1} + a f_i\Big]. \end{aligned} \tag{15}$$

Then, the λ_s and μ_s coefficients are

$$\{\lambda_s | s = 0, \ldots, 5\} = \{-\beta, -(\alpha - \beta), -(1-\alpha), 1-\alpha, \alpha - \beta, \beta\},$$
$$\{\mu_s | s = 0, \ldots, 5\} = \{a, b, c, d, e, g\}.$$

Equation (15) is a 5-step method which will be implicit in a general nonlinear case where f depends on F, as long as $g \neq 0$. In the limit case of $\beta = 0$, the method is 3-step, i.e.,

$$\alpha F_{i+3} + (1-\alpha)F_{i+2} - (1-\alpha)F_{i+1} - \alpha F_i = h\Big[ef_{i+3} + df_{i+2} + cf_{i+1} + bf_i\Big], \quad (16)$$

where

$$\{\lambda_s | s = 0, \ldots, 3\} = \{-\alpha, -(1-\alpha), 1-\alpha, \alpha\},$$
$$\{\mu_s | s = 0, \ldots, 3\} = \{b, c, d, e\}.$$

To keep the same number of points in the left- and right-hand side, $a = g = 0$ has been taken. Additionally, if $e \neq 0$ then (16) is an implicit method. The coefficients $\{\alpha, \beta\}$ and parameters $\{a, b, c, d, e, g\}$ are those in Table 1. As any CIR scheme can be cast as a linear multistep method one may wonder at this point if there is any reason to implement CIR as a multistep method instead of a tri/penta-diagonal system. Of course, this will depend on the characteristics of multistep CIR, so in the following subsections the consistency and stability of a multistep CIR of three or five steps will be checked.

5.1. Consistency

A linear multistep method is consistent if the truncation error defined as

$$TE_i = \frac{\sum_{s=0}^{m} \left(\lambda_s F_{i+s} - h\mu_s F'_{i+s}\right)}{h\sum_{s=0}^{m} \mu_s},$$

tends to zero when the space length h tends to zero as well. TE_i is divided by $h\sum_{s=0}^{m} \mu_s$ in order to normalize the error. In terms of the first, $\rho(r) = \sum_{s=0}^{m} \lambda_s r^s$, and second, $\sigma(r) = \sum_{s=0}^{m} \mu_s r^s$, characteristic polynomials the condition reads

$$\rho(1) = 0 \qquad \text{and} \qquad \rho'(1) = \sigma(1) \neq 0. \quad (17)$$

For the 5-step CIR these two polynomials are

$$\rho_5(r) = \beta r^5 + (\alpha - \beta)\, r^4 + (1-\alpha)r^3 - (1-\alpha)r^2 - (\alpha - \beta)r - \beta,$$
$$\sigma_5(r) = gr^5 + er^4 + dr^3 + cr^2 + br + a,$$

whereas for the 3-step CIR

$$\rho_3(r) = \alpha r^3 + (1-\alpha)r^2 - (1-\alpha)r - \alpha,$$
$$\sigma_3(r) = er^3 + dr^2 + cr + b.$$

The first condition in (17) is met because terms containing α and β cancel out, whereas the second condition yields the equation (5). Therefore a 3-step CIR is consistent if $\alpha \neq -1/2$ and so is 5-step CIR is if $\alpha + \beta \neq -1/2$. As none of the CIR schemes put forward in the previous section, e.g. (9), (10) and (11), have negative values of $\{\alpha, \beta\}$, the condition is satisfied.

5.2. Stability

Aside from consistency, stability plays an important role in the numerical analysis. The theory of linear multistep method distinguishes two types of stabilities: Zero- and A-stability. A method is called zero-stable if the numerical solution

$$\sum_{s=0}^{m} \lambda_s F_{i+s} = 0,$$

remains bounded as $i \to \infty$, or roughly speaking, round-off errors do not grow up. That is checked by the roots of the first characteristic polynomial which must lie within a unit circle with at most a simple root on the edge of the disk. For instance, the polynomial $\rho_3(r)$ can be factorized as

$$\rho_3(r) = (r-1)\left(\alpha r^2 + r + \alpha\right).$$

The first root has $|r_0| = 1$. If r_1, r_2 are the roots of $\alpha r^2 + r + \alpha$, then

$$\begin{cases} r_1 + r_2 = -1/\alpha, \\ r_1 r_2 = 1. \end{cases}$$

The second equation of the system tells that if one solution, e.g., $|r_1| \leq 1$ then $|r_2| \geq 1$ $\forall \alpha$. Similarly with the 5-step CIR,

$$\rho_5(r) = (r-1)\left(\beta r^4 + \alpha r^3 + r^2 + \alpha r + \beta\right),$$

one root is on the unit disk and the others obey

$$\begin{cases} r_1 + r_2 + r_3 + r_4 = -\alpha/\beta, \\ r_1 r_2 + r_2 r_3 + r_3 r_4 + r_4 r_1 + r_1 r_3 + r_2 r_4 = 1/\beta, \\ r_1 r_2 r_3 + r_2 r_3 r_4 + r_1 r_2 r_4 + r_1 r_3 r_4 = -\alpha/\beta, \\ r_1 r_2 r_3 r_4 = 1, \end{cases}$$

where at least one root will be outside the disk. Therefore, the CIR method as a linear multistep method is not stable, it is mandatory that the integrals related to CIR be solved by a tri/pentadiagonal matrix system.

5.3. Build an ODE solver with CIR

As seen in previous section, CIR, written as a multistep method does not have good stability properties but written as a system of equations is able to numerically approximate ODEs. Let us consider for instance the nonhomogeneous linear BVP

$$\begin{cases} y'(x) + p(x)y(x) = q(x), \quad x_0 \le x \le x_N, \\ y(x_0) = y_{\text{BC}}, \end{cases} \tag{18}$$

being y_{BC} a given value at the boundary. The CIR method can be applied to y' with, e.g., rule (9) in the following manner

$$\begin{aligned} \frac{1}{10}\int_{x_{i-2}}^{x_{i-1}} y'\,\mathrm{d}x + \int_{x_{i-1}}^{x_i} y'\,\mathrm{d}x + \frac{1}{10}\int_{x_i}^{x_{i+1}} y'\,\mathrm{d}x &= \frac{3\,h}{5}\left(y'_{i-1} + y'_i\right), \\ \frac{y_{i-1} - y_{i-2}}{10} + y_i - y_{i-1} + \frac{y_{i+1} - y_i}{10} &= \frac{3\,h}{5}\left(q_{i-1} + q_i\right) - \\ & \quad \frac{3\,h}{5}\left(p_{i-1}y_{i-1} + p_i y_i\right). \end{aligned}$$

Grouping the terms y_{i-1} and y_i, a four-point stencil for the discrete solution $\{y_i\}$ at inner points reads

$$-\frac{1}{10}y_{i-2} + \left(\frac{3h}{5}p_{i-1} - \frac{9}{10}\right)y_{i-1} + \left(\frac{3h}{5}p_i + \frac{9}{10}\right)y_i + \frac{1}{10}y_{i+1} = \frac{3h}{5}\left(q_{i-1} + q_i\right).$$

As for the boundary schemes, the boundary expressions are employed with order 5 and $\alpha = 1$ in table 2,

$$\left(\frac{h}{3}p_0 - 1\right) y_0 + \frac{4h}{3}p_1 y_1 + \left(\frac{h}{3}p_2 + 1\right) y_2 = \frac{h}{3}\left(q_0 + 4q_1 + q_2\right),$$
$$\left(\frac{h}{3}p_{N-2} - 1\right) y_{N-2} + \frac{4h}{3}p_{N-1} y_{N-1} + \left(\frac{h}{3}p_N + 1\right) y_N = \frac{h}{3}\left(q_{N-2} + 4q_{N-1} + q_N\right),$$

Thus, the numerical solution is achieved by solving

$$\mathbf{M}\mathbf{y} = h\mathbf{M_2}\mathbf{q} + \mathbf{y}_{\text{BC}}, \quad \mathbf{M} = \mathbf{M}_1 + h\mathbf{M}_2\,\text{diag}(\mathbf{p}),$$

where the vectors are defined as

$$\mathbf{y} = (y_0, y_1, \ldots, y_N)^T, \quad \mathbf{y}_{\text{BC}} = (y_{\text{BC}}, 0, \ldots, 0)^T,$$
$$\mathbf{p} = (p_0, p_1, \ldots, p_N)^T, \quad \mathbf{q} = (q_0, q_1, \ldots, q_N)^T,$$

and the matrices

$$\mathbf{M}_1 = \begin{pmatrix} 1 & 0 & 0 & \cdots & \cdots & \cdots & 0 \\ -1 & 0 & 1 & \ddots & \ddots & \ddots & \vdots \\ -\frac{1}{10} & -\frac{9}{10} & \frac{9}{10} & \frac{1}{10} & \ddots & \ddots & \vdots \\ 0 & -\frac{1}{10} & -\frac{9}{10} & \frac{9}{10} & \frac{1}{10} & \ddots & \vdots \\ \vdots & \ddots & \ddots & \ddots & \ddots & \ddots & 0 \\ \vdots & \ddots & \ddots & -\frac{1}{10} & -\frac{9}{10} & \frac{9}{10} & \frac{1}{10} \\ 0 & \cdots & \cdots & 0 & -1 & 0 & 1 \end{pmatrix},$$

$$\mathbf{M}_2 = \begin{pmatrix} 0 & 0 & 0 & \cdots & \cdots & \cdots & 0 \\ \frac{1}{3} & \frac{4}{3} & \frac{1}{3} & \ddots & \ddots & \ddots & \vdots \\ 0 & \frac{3}{5} & \frac{3}{5} & 0 & \ddots & \ddots & \vdots \\ \vdots & 0 & \frac{3}{5} & \frac{3}{5} & 0 & \ddots & \vdots \\ \vdots & \ddots & \ddots & \ddots & \ddots & \ddots & 0 \\ \vdots & \ddots & \ddots & 0 & \frac{3}{5} & \frac{3}{5} & 0 \\ 0 & \cdots & \cdots & 0 & \frac{1}{3} & \frac{4}{3} & \frac{1}{3} \end{pmatrix}.$$

Should greater accuracy be required, e.g., the rule with $\alpha = 27/11$ could be used. The $\mathbf{M}_1$, $\mathbf{M}_2$ banded matrices would change to

$$\mathbf{M}_1 = \begin{pmatrix} 1 & 0 & 0 & \cdots & \cdots & \cdots & 0 \\ -1 & -\frac{16}{11} & \frac{27}{11} & \ddots & \ddots & \ddots & \vdots \\ -11 & -27 & 27 & 11 & \ddots & \ddots & \vdots \\ 0 & -11 & -27 & 27 & 11 & \ddots & \vdots \\ \vdots & \ddots & \ddots & \ddots & \ddots & \ddots & 0 \\ \vdots & \ddots & \ddots & -11 & -27 & 27 & 11 \\ 0 & \cdots & \cdots & 0 & -\frac{27}{11} & \frac{16}{11} & 1 \end{pmatrix},$$

$$\mathbf{M}_2 = \begin{pmatrix} 0 & \cdots & \cdots & \cdots & \cdots & \cdots & 0 \\ \frac{281}{990} & \frac{1028}{495} & \frac{196}{165} & -\frac{52}{495} & \frac{1}{90} & \ddots & \vdots \\ 3 & 27 & 27 & 3 & 0 & 0 & \vdots \\ 0 & 3 & 27 & 27 & 3 & \ddots & \vdots \\ \vdots & \ddots & \ddots & \ddots & \ddots & \ddots & 0 \\ \vdots & 0 & 0 & 3 & 27 & 27 & 3 \\ 0 & \cdots & \frac{1}{90} & -\frac{52}{495} & \frac{196}{165} & \frac{1028}{495} & \frac{281}{990} \end{pmatrix}.$$

Two numerical cases are proposed. The first one is a homogeneous, $q(x) = 0$, linear BVP with variable coefficient, $p(x) = 2x$, and boundary condition $y(0) = 1$ whose exact solution is the Gaussian function, $y(x) = e^{-x^2}$. The other case is a stiff problem with $p(x) = 1000$, $q(x) = 3000 - 2000e^{-x}$ and $y(0) = 0$. Its exact solution takes the form

$$y(x) = 3 - \frac{997e^{-1000\,x} + 2000e^{-x}}{999},$$

and describes a process with two characteristic length scales as shown below in figure 7a.

In both cases the L_2-norm of the vector difference between the numerical

solution and the exact one was computed. The system of equations for both cases was calculated in Matlab with one of Lapack solvers for banded matrices. The numerical solution of CIR was compared with two versions of a Predict-Evaluate-Correct-Evaluate (PECE) multistep method. This method was also coded in Matlab.

- Predictor with an Adams-Bashforth four-, five-step (AB4, AB5)
- Corrector with an Adams-Moulton three-, four-step (AM3, AM4)

Clearly, 4th-order CIR is slightly better than AB4-AM3 and both reach 4th-order accuracy. In contrast, the AB5-AM4 method is 5th-order, whereas 6th-order CIR attains the theoretical order of accuracy.

The initial strong variation of the stiff problem makes the CIR schemes not so practical in this case if h is constant. Due to the two distinct characteristic lengths a function $h = h(x)$ is needed, but CIR is derived with h constant. The solution is to define a break point, x_b thereby a constant h_1 is used within the interval $[x_0, x_b]$ whereas a constant h_2 is adopted in the interval $[x_b, x_N]$, being $h_1 < h_2$. The link between the two zones is x_b where the equations for the boundaries are employed.

As in the Gaussian problem, system CIR achieves 4th-, 6th-order accuracy, see figure 7b. $\overline{h}$ stands for average interval length. For the variable step-size PECE method with tolerance 10^{-4}, $h_{\min} = 10^{-5}$ and $h_{\max} = 10^{-2}$, the L_2-norm was $4.41 \cdot 10^{-5}$ with $\overline{h} = 1.4 \cdot 10^{-3}$. For the same $\overline{h}$ the 4th-order CIR gives a L_2-norm of 10^{-8} and the sixth-order, 10^{-12}.

As already commented CIR cast as multistep method is unstable. It was verified for both ODE problems that this was in fact the case.

6. Numerical Examples

Some numerical tests have been set up for checking how accurate CIR is for numerical integration. Eventually, 4th-order rule (9), 6th-order rule (10),

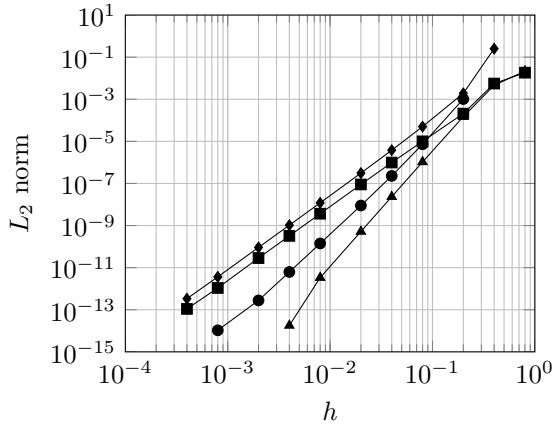

Figure 6: Linear ODE $y' + 2xy = 0$; $y(0) = 1$. **Black Square**, 4th-order rules; **Black Triangle**, 6th-order rules; **Black Diamond**, AB4-AM3; **Black Circle**, AB5-AM4.

8th-order rule (11) and their equal-order boundary rules, have been used. Notice that in all cases the matrix is tridiagonal, therefore one may apply direct methods for solving the algebraic system such as TDMA.

The range of applications is wide. Although we were mainly interested in the application of the integration rules for the calculation of the integrals in the ENATE coefficients [12], several, and very different, applications were dealt with to show the general applicability of the method.

6.1. Data set

The compact numerical integration will be first checked with a very simple mathematical problem: the total distance traveled by a car given its velocity at different times. The car velocity follows the function

$$v\left(t\right) = \frac{4}{15} \begin{cases} 3t^2 & t \in [0,5]\,\mathrm{s}, \\ 100 - t^2 & t \in [5,10]\,\mathrm{s}, \end{cases}$$

whose exact integration yields $\mathrm{D} = \int_0^{10} v\left(t\right) \mathrm{d}t = 88.\overline{8}\,\mathrm{m}$. Now let us assume that this equation is unknown and only a short data set is available provided in

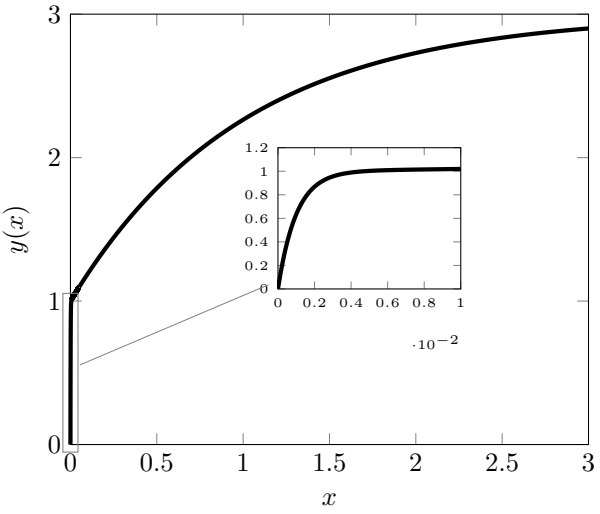

(a) Exact solution.

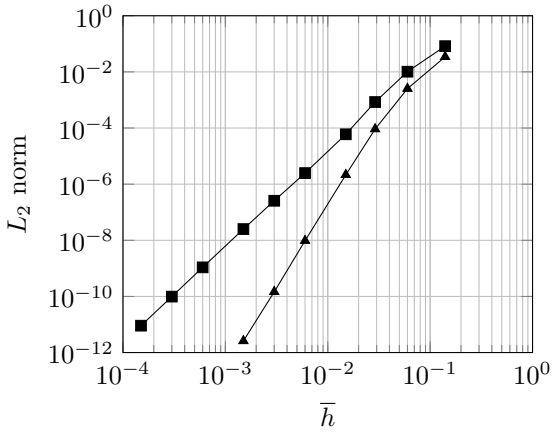

(b) **Black Square**, 4th-order rules; **Black Triangle**, 6th-order rules.

Figure 7: Linear ODE $y' + 1000y = 3000 - 2000e^{-x}$; $y(0) = 0$.

i	t_i s	$v(t_i)$ m/s
0	0	0
1	2.5	5
2	5	20
3	7.5	$11.\overline{6}$
4	10	0

Table 8: Data set of velocities and times.

Table 8. The composite Trapezoidal rule and 4th-order compact rule were used in order to show up the differences. The results are displayed in Table 9.

	Rule	
	2th	4th
D	91.25 m	$88.\overline{8}$ m

Table 9: The total distance traveled.

Although the composite Simpson's rule could have also been used with the same results as the 4th-order rule,

$$\int_0^{10} v\,(t)\,\mathrm{d}t \simeq \frac{h}{3}\Big[v(t_0) + 4v(t_1) + 2v(t_2) + 4v(t_3) + v(t_4)\Big] = 88.\overline{8}\,\mathrm{m},$$

it can only work if the global domain is split up in a even number of intervals. The compact integrals do not have this limitation.

6.2. The simple pendulum

In this section, the period of a simple pendulum as that pictured in Figure 8 was chosen as a test for CIR. A simple pendulum consists of a bob of mass m attached to a massless string of length l under a gravity field g. Friction with junctions and air was disregarded. The changes of the angular displacement, $\theta\,(t)$, of the pendulum is described by a non-linear second order ODE,

$$\theta'' + \frac{g}{l}\sin\theta = 0,$$

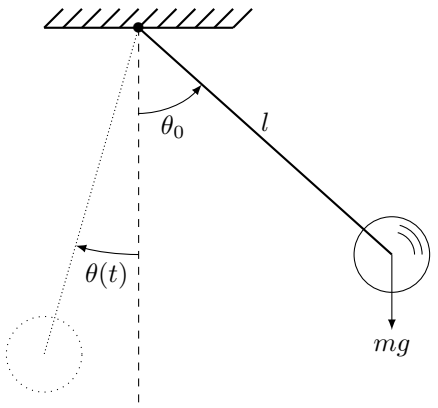

Figure 8: The simple pendulum.

with $\theta\,(t=0)=\theta_0$ and $\theta'\,(t=0)=0$ as initial values. Therefore, the period T, which is the time that takes the bob mass in recovering the initial position in one cycle is

$$T = 4\sqrt{\frac{l}{2g}}K(k) \quad \text{with} \quad K(k) = \int_0^{\pi/2} \frac{\mathrm{d}u}{\sqrt{1-k^2\sin^2 u}},$$

where K is the complete elliptic integral of the first kind and $k = \sin(\theta_0/2)$ is the elliptic modulus or eccentricity. On the other hand K could be expressed in terms of an infinite series,

$$K(k) = \frac{\pi}{2}\sum_{m=0}^{\infty}\left[\frac{(2m-1)!!}{(2m)!!}\right]^2 k^{2m},$$

with the mark !! denoting the double factorial. A twenty-term series of this expression was considered the exact solution as it was accurate enough for the amplitudes that were tested. In the first numerical case, Figure 9a, $\theta_0 = 10^\circ \equiv \pi/18\,rad$ was used as representative of a low amplitude pendulum for which $\sin\theta \approx \theta$ and therefore $K \approx \pi/2$. In Figure 9b, θ_0 was $60^\circ \equiv \pi/3\,rad$. The absolute value of the difference between the calculated period and the exact one is plotted.

As is shown in the convergence plots, either 4th- or 6th-order rules worked mostly one order of magnitude better than in theory. The low amplitude case

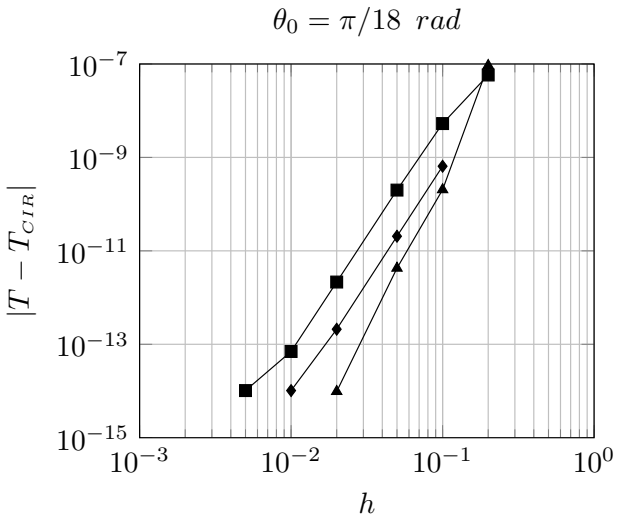

(a) Pendulum with a low amplitude

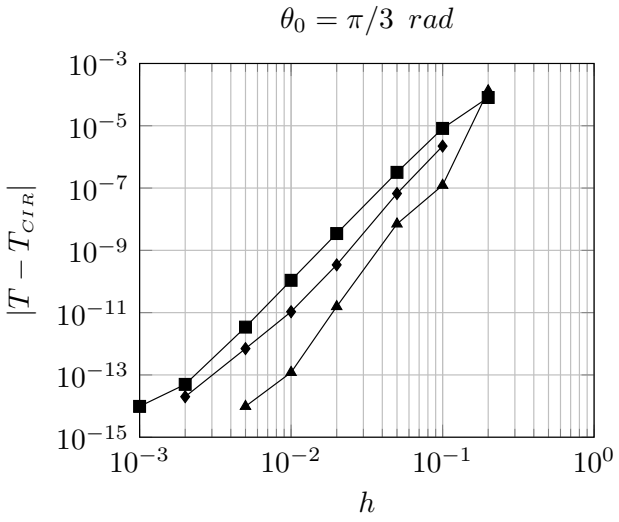

(b) Pendulum with a great amplitude

Figure 9: Convergence plots for two different θ_0: **Black Square**, 4th-order rule; **Black Triangle**, 6th-order rule; **Black Diamond**, 8th-order rule.

reached machine accuracy with an interval length h of $2 \cdot 10^{-2}$ with the best scheme whereas in the large amplitude case, $h = 5 \cdot 10^{-3}$ was required. Surprisingly, the 8th-order rule was found to have an error norm roughly one order of magnitude higher than 6th-order rule, behaving like the 4th-order rule. It was thought that the round-off errors were influential in the behaviour of 8th-order rule results but against this hypothesis was the fact that the error did not depend on the number of computer operations of the direct solver as the results obtained by another direct solver were the same.

CIR results with 5 nodes were compared with other integration rules such as those written at the beginning of the paper, where the number of nodes employed by each is indicated. They are shown in table 10. As seen in the table, CIR calculates the integral with an error similar to other rules although it must be stressed that CIR does not show all its potential with large interval sizes. It requires a greater number of intervals to reach the asymptotic order of accuracy.

Rule	Low amplitude	Great amplitude
Simpson	$2.5826 \cdot 10^{-6}$	$3.8833 \cdot 10^{-3}$
Boole	$1.7217 \cdot 10^{-7}$	$2.4314 \cdot 10^{-4}$
Gauss 2 points	$1.8643 \cdot 10^{-6}$	$2.7958 \cdot 10^{-3}$
Gauss 3 points	$1.7396 \cdot 10^{-7}$	$2.4124 \cdot 10^{-4}$
Cubic Hermite	$7.7480 \cdot 10^{-6}$	$1.1827 \cdot 10^{-2}$
Quintic Hermite	$2.6500 \cdot 10^{-6}$	$3.9568 \cdot 10^{-3}$
CIR 4th order	$5.8069 \cdot 10^{-8}$	$8.0734 \cdot 10^{-5}$
CIR 6th order	$9.2833 \cdot 10^{-8}$	$1.3308 \cdot 10^{-4}$

Table 10: Pendulum test, errors for several quadrature rules.

6.3. Integral transforms

The first uses of integral transforms went back to the Fourier series in 1822 and Laplace on probability theory in 1812. The key strategy consists of transforming the original problem, that a priori is difficult to solve, into another whose domain, that does not need to match with the original, makes it easier. There are a plenty of integral transforms such as Fourier, Laplace, Abel, Hilbert, among others (for further information see Davies [13]). On the whole, an integral transform is written as

$$\mathcal{IT}\left[f(t)\right](m) = \int_{t_0}^{t_1} K(m,t) f(t)\,\mathrm{d}t,$$

where $K(m,t)$ is called *the kernel* and t_0, t_1 are the limits of integration. Focusing the study on the Laplace transform, $K(s,t) = e^{-st}$, $t_0 = 0$ and $t_1 \to \infty$. It is an improper integral of first kind, so instead of taking the limit as

$$\mathcal{L}\left[f(t)\right](s) = \lim_{a\to\infty} \int_0^a e^{-st} f(t)\,\mathrm{d}t,$$

that only complicates the numerical problem, it is advisable to change the limits of the integral in order to discretize it in a finite domain. In that case, the change of variables $t = u/(1-u)$ with $u \in [0,1]$ can be applied to reach this goal,

$$\mathcal{L}\left[f(t)\right](s) = \int_0^1 \frac{e^{-s\,u/(1-u)}}{(1-u)^2} f\left(t(u)\right)\,\mathrm{d}u.$$

The integrand has two variables: the variable of integration u, and s, that remains constant in the integral. So, for each value of s it will be necessary to work out the previous integral. The Laplace transform of two functions, a Heaviside step and a damped cosine wave will be calculated. The expressions are shown below. For both Heaviside steps, $t_0 = 0$ s and $t_0 = 2$ s, 20 values of s were considered from 0.1 to 2, and for the damped cosine wave 101 values of s were calculated, from 0 to 10.

$$f(t) = \mathcal{H}(t - t_0) = \begin{cases} 0 & t < t_0 \\ 1 & t \geq t_0 \end{cases} \quad \rightarrow \quad \mathcal{L}\left[f(t)\right](s) = \frac{e^{-t_0\, s}}{s},$$

$$f(t) = e^{-t}\cos(2t) \quad \rightarrow \quad \mathcal{L}\left[f(t)\right](s) = \frac{s+1}{s^2+2s+5}.$$

As usual, the L_2-norm will be used as accuracy indicator. Some remarkable outcomes were observed. First, for the damped cosine wave all rules give roughly the same norms in the region of $h > 10^{-2}$, figure 10, and they start to spread out for smaller h. The 6th-order rule reaches machine accuracy very quickly, in one decade decreases 10 orders of magnitude. It works much better than it would be theoretically foreseeable.

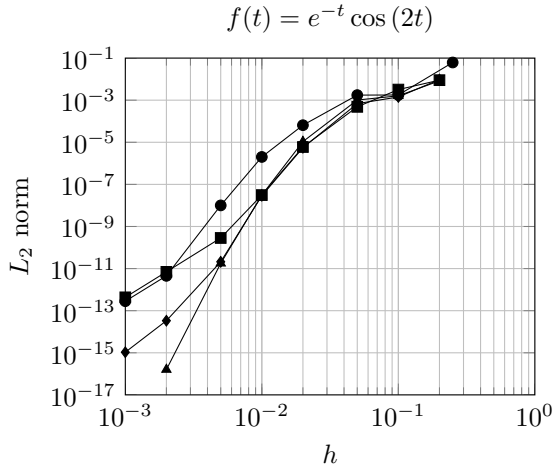

Figure 10: Convergence plot for the Laplace transform of a damped cosine wave: **Black Square**, 4th-order rule; **Black Triangle**, 6th-order rule; **Black Diamond**, 8th-order rule; **Black circle**, Composite Simpson Rule.

Both Laplace transforms, Figures 10 and 11, displayed a similar behaviour. In the first decade of h almost all rules provided similar norms with slight oscillations. In the case of the Heaviside step the 4th-order CIR displayed lower norm than the others below $h \sim 10^{-2}$. This behaviour was somehow unexpected and the reason is still unknown to us. The Laplace transform of the Heaviside

step is difficult to integrate for small s due to rhe shape of the integrand. In Figure 12 several integrands with different s are depicted. As s increases the integrand turns into a spiky function difficult to integrate for all CIR.

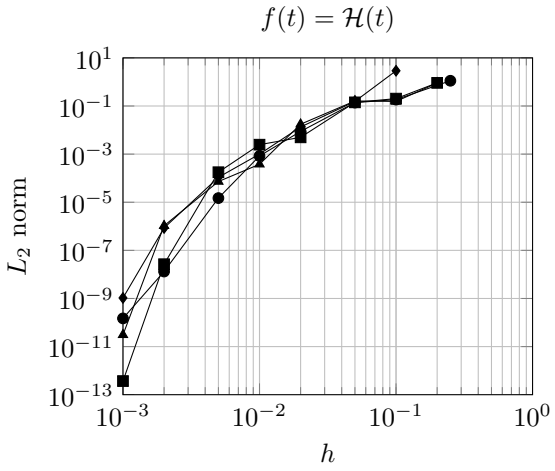

(a) Without a time delay gap.

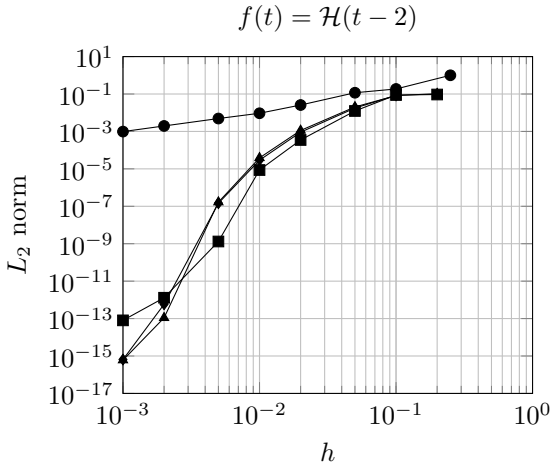

(b) With a time delay gap.

Figure 11: Convergence plots for the Laplace transform of a Heaviside unit step: same notation as Figure 10.

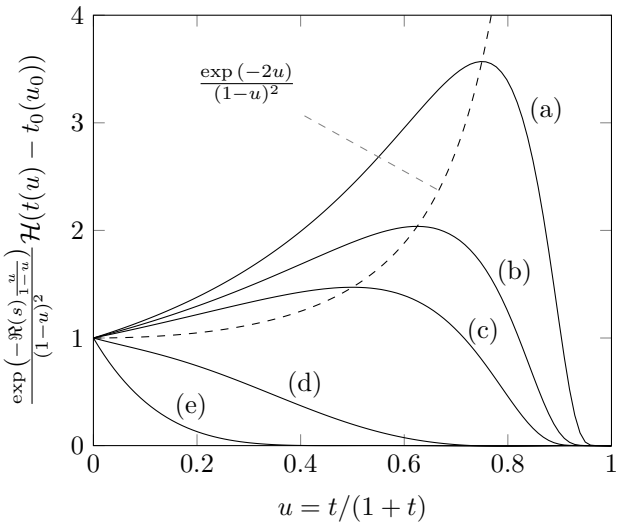

Figure 12: Representation in modulus of Laplace's integrand for the Heaviside function with several values of the real part: (a) $\Re(s) = 0.5$, (b) $\Re(s) = 0.75$, (c) $\Re(s) = 1$, (d) $\Re(s) = 3$, and (e) $\Re(s) = 10$. The dashed line is the path of the maximum that rises quickly for $\Re(s) < 1$ what produces a spiked function tough to integrate.

Again the two CIR were compared with other integration rules in table 11. In the Heaviside step, similar errors were obtained with CIR and Gauss. The bad resolution of Hermite is caused by the difficulty of Hermite splines to fit an integrand with strong variations. In the damped cosine wave, CIR improved slightly the results followed by Gauss 3 points and Boole.

6.4. The 2D pure-convection transport equation

Finally, the last application is related to a new way of discretizing a generic convection-diffusion equation proposed by one of the authors, see Pascau [14] and Pascau et al [12]. The new scheme is exact in a one-dimensional case with a three-point stencil as long as the integrals contained in the coefficients can be calculated exactly. In a general case these will have to be obtained numerically and this is in fact the reason why we started looking at ways of evaluating the integrals with the compact integration rules.

Let us briefly consider ENATE in a 2D pure convection case chosen as a

Rule	Heaviside step		Damped cosine wave
	$t_0 = 0$ s	$t_0 = 2$ s	
Simpson	1.8353	$6.7536 \cdot 10^{-1}$	$1.3212 \cdot 10^{-1}$
Boole	1.0764	$7.7421 \cdot 10^{-2}$	$7.3119 \cdot 10^{-2}$
Gauss 2 points	$5.3457 \cdot 10^{-1}$	$6.0942 \cdot 10^{-1}$	$1.0274 \cdot 10^{-1}$
Gauss 3 points	$5.4519 \cdot 10^{-1}$	$2.3136 \cdot 10^{-1}$	$4.7186 \cdot 10^{-2}$
Cubic Hermite	2.5312	1.6068	$1.9214 \cdot 10^{-1}$
Quintic Hermite	2.4997	1.5646	$1.1505 \cdot 10^{-1}$
CIR 4th order	$9.1453 \cdot 10^{-1}$	$9.3967 \cdot 10^{-2}$	$8.9138 \cdot 10^{-3}$
CIR 6th order	$9.0122 \cdot 10^{-1}$	$1.0411 \cdot 10^{-1}$	$8.2745 \cdot 10^{-3}$

Table 11: Laplace transform test, L_2-norm for several quadrature rules.

test,

$$
\begin{aligned}
&u\frac{\partial u}{\partial x} + u\frac{\partial u}{\partial y} = S, \quad (x, y) \in [0, 1] \times [0, 1], \\
&u(x, 0) = a + \sin(x - 0.5), \quad \text{on } y = 0, \;\; 0 \leq x \leq 1, \\
&u(0, y) = b + \tanh(\sigma(y - 0.5)), \quad \text{on } x = 0, \;\; 0 \leq y \leq 1,
\end{aligned}
$$

where $a = 2 + \tanh(-\sigma \cdot 0.5)$ and $b = 2 + \sin(-0.5)$. This is a 2D steady Burgers' equation in which the velocity components are the same, so there is only one PDE to solve. We employ a manufactured source with a parameter that controls the steepness of the solution in a certain desired region,

$$
S = \left(\frac{\sigma}{\cosh^2(\sigma(y - 0.5))} + \cos(x - 0.5) \right) (\tanh(\sigma(y - 0.5)) + 2 + \sin(x - 0.5)).
$$

The exact solution is

$$
u = \tanh(\sigma(y - 0.5)) + 2 + \sin(x - 0.5),
$$

which is very anisotropic, the gradient of u does not change alike in both directions. The sine function in one direction is very smooth but the sharpness of the hyperbolic tangent function is controlled by σ, an input parameter. In fact, the greater the value of σ is, the greater the gradient of u in y-direction around 0.5 becomes, see Figure 13.

ENATE works with the conservative form of the transport equation, i.e.,

$$\frac{\partial\left(\rho u\phi\right)}{\partial x}+\frac{\partial\left(\rho u\phi\right)}{\partial y}=S,$$

where the conserved variable is the variable under study, $\phi = u$ and $\rho = 1/2$. The convective term uses the values of u in the previous iteration, $\rho u = [u/2]^{\text{old}}$. The product $\rho u\phi$ is the total flux J. The target PDE is split up into two ODEs such as in Wong et al. [15], by setting the derivatives in the other directions as new source terms,

$$\frac{\partial\left(\rho u\phi\right)}{\partial x}=S-\frac{\partial J}{\partial y},$$
$$\frac{\partial\left(\rho u\phi\right)}{\partial y}=S-\frac{\partial J}{\partial x}.$$

The final nodal equation is obtained by using a uniform discretization, integrating both equations along their coordinates

$$(\rho u)_P\phi_P=(\rho u)_W\phi_W+IS_{WP}-\int_W^P\frac{\partial J}{\partial y}\mathrm{d}x,$$
$$(\rho u)_P\phi_P=(\rho u)_S\phi_S+IS_{SP}-\int_S^P\frac{\partial J}{\partial x}\mathrm{d}y,$$

and adding them up

$$2\left(\rho u\right)_P\phi_P=\left(\rho u\right)_W\phi_W+\left(\rho u\right)_S\phi_S+IS_{WP}+IS_{SP}-\left[\int_W^P\frac{\partial J}{\partial y}\mathrm{d}x+\int_S^P\frac{\partial J}{\partial x}\mathrm{d}y\right]^{\text{old}},\tag{19}$$

where IS_{ab} stands for Integral of the Source term within $[a, b]$. A finite volume formulation was used where W stands for west-, S, south-, and P, central-node. The main issue are the unknown $\partial_i J$ integrals as the procedure only

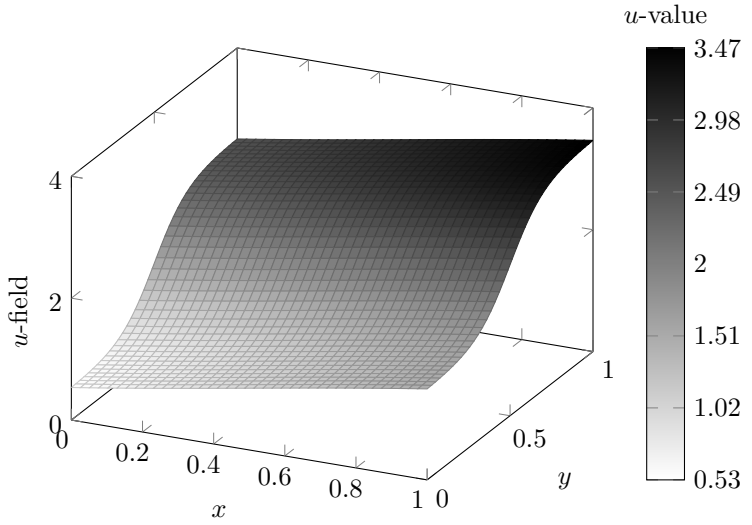

(a) Smooth gradient - $\sigma = 5$

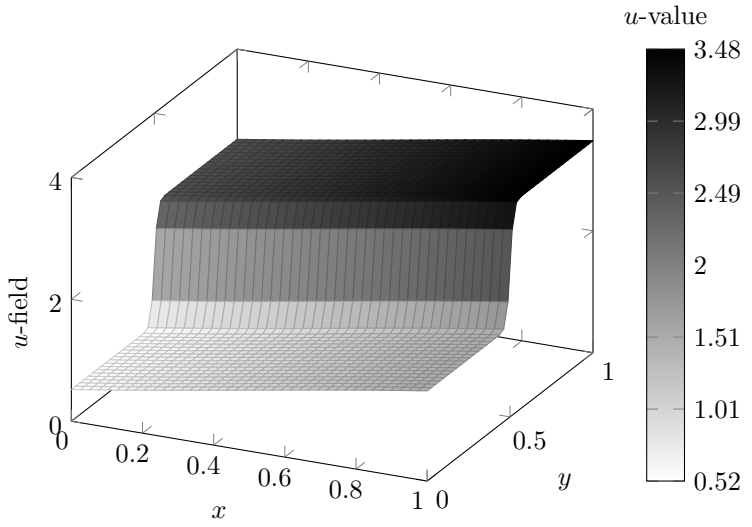

(b) Sharp gradient - $\sigma = 50$

Figure 13: Exact solution of the transport equation using the manufactured source.

provides the value of u in each iteration and node. To obtain J is immediate but in addition, and unlike the numerical examples discussed above, the integral values in each interval of the mesh are required in this example. CIR can provide these integrals at once but prior to this the values of the integrands, that is, J derivatives, are necessary. A central finite difference scheme could have been chosen, although the accuracy is only second-order that can mask the higher accuracy of CIR. A central compact scheme (CCS), as in Lele [1], was picked since it provides low dispersion/diffusion errors, see Boersma [16]. The strategy carried out is displayed in Figure 14. The domain is swept in both directions line-by-line from left to right and from bottom to top. The contribution of the adjacent line (South from bottom to top and West from left to right) is moved to the source term. Let us take, for instance, the sweep from bottom to top where horizontal lines are calculated. The calculation along y-constant lines is

$$2\left(\rho u\right)_P \phi_P \quad = \quad \left(\rho u\right)_W \phi_W + \text{Source terms.}$$

All remaining terms of equation (19) are included in "Source terms". The main difficulty lies in the evaluation of the $\partial_y J$ integral and the $\partial_x J$ integral. As an example, to evaluate the $\partial_y J$ integral, the procedure can be summarized as follows:

1. Calculate $J = u^2/2$
2. Use CCS line-by-line in order to evaluate $\partial J/\partial y$ along x=constant lines,
3. Use CIR line-by-line in order to evaluate $\int(\partial J/\partial y)\mathrm{d}x$ along y=constant lines,
4. The $\partial_y J$ integral in each sub-interval is ready to be used in the algebraic equation.

The code was run until the difference between two consecutive iterations was less than 10^{-4}. The transport equation has been further discretized with another numerical scheme named "Finite Volume-Complete Flux" (FV-CF), [17], since it has a similar flavour to ENATE and moreover, both have already been compared in a one-dimensional case, [18]. As is remarked by its authors,

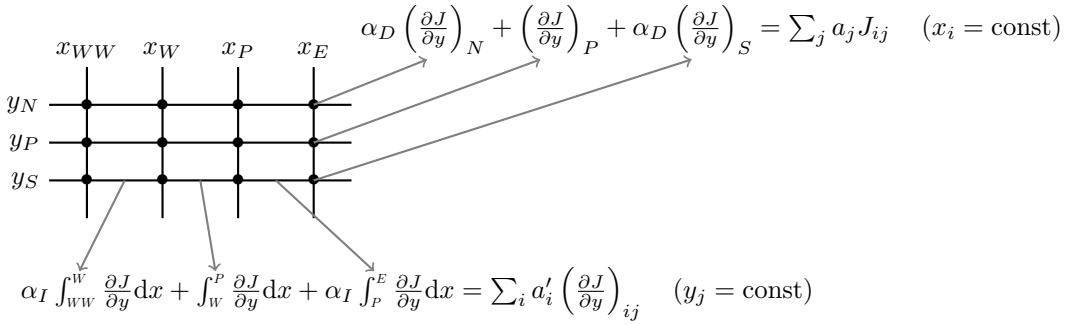

Figure 14: Simplified representation for evaluating the $\partial_y J$ integral in an uniform grid. Similar procedure for $\partial_x J$ integral. The parameters of CCS, α_D, and CIR, α_I, do not have to be the same.

FV-CF scheme becomes a second-order cell-vertex FV method when Péclet goes to infinity, as in this example.

Next, the L_2-norm is plotted in Figure 15 where eight numerical experiments were implemented: two levels in the gradient and four CIR/CCS combinations. Both smooth and sharp gradient simulations using a 4th-order CIR + 4th-order CCS, 6th-order CIR + 4th-order CCS showed an identical behaviour. In both cases, ENATE worked as 4th-order scheme, Table 12, being slightly better with a smooth gradient.

The 4th-order CIR + 6th-order CCS and 6th-order CIR + 6th-order CCS follow the same behaviour in sharp gradient, except for the 500 $\times$ 500 mesh whose results differ each other less than one order of magnitude. ENATE worked as 6th-order. With a smooth gradient and same orders of CIR and CCS the differences became relevant beyond the 200 $\times$ 200 mesh. Rejecting results of the non-asymptotic zone, 4th-order ENATE was achieved with a 4th-order CIR + 6th-order CCS and 6th-order ENATE was obtained by 6th-order CIR + 6th-order CCS. On the other hand, 8th-order CIR or CCS did not provide good results and they are not reported.

It is worth highlighting the good results obtained by ENATE with its accessories (CCS and CIR) in a nonlinear equation. In the more stringent case of

$\sigma = 50$ the L_2-norm is $3 \cdot 10^{-10}$ with a mesh 500×500.

ENATE provides much better results than the FV-CF scheme, even for the case $\sigma = 50$ that contains a region where the solution changes very quickly. ENATE cannot provide a solution for $\sqrt{\Delta x \Delta y} > 2 \cdot 10^{-2}$ whereas FV-CF can work fine for $\sqrt{\Delta x \Delta y}$ greater than this value. For large $\sqrt{\Delta x \Delta y}$ ENATE is more sensitive to nonlinearities than the FV-CF scheme.

Case	σ	CIR	CCS	ENATE	Remarks
1.1	5 (Smooth)	4th	4th	4th	
1.2		4th	6th	4th	better than 1.1
1.3		6th	4th	4th	identical to 1.1
1.4		6th	6th	6th	
2.1	50 (Sharp)	4th	4th	4th	
2.2		4th	6th	6th	
2.3		6th	4th	4th	identical to 2.1
2.4		6th	6th	6th	

Table 12: Orders obtained by several combinations of CCS and CIR.

7. Conclusions

The purpose of the current paper was to carry out an easy-to-use numerical procedure to determine the definite integral of a function. Once the integration domain has been split up uniformly, the method consists of solving an algebraic system of equations where the components of the vector of unknowns are the definite integrals over each interval. The independent vector contains a linear combination of the function values in the discrete points. The matrix is banded with coefficients which keep relationship with the weights of the linear combination by matching derivatives in Taylor's coefficients. Special attention must be paid at both boundary and next to boundary points. Were it necessary to change the order of the approximation, it would be as easy as changing the values of this parameters and weights. Furthermore, it could be noticed that

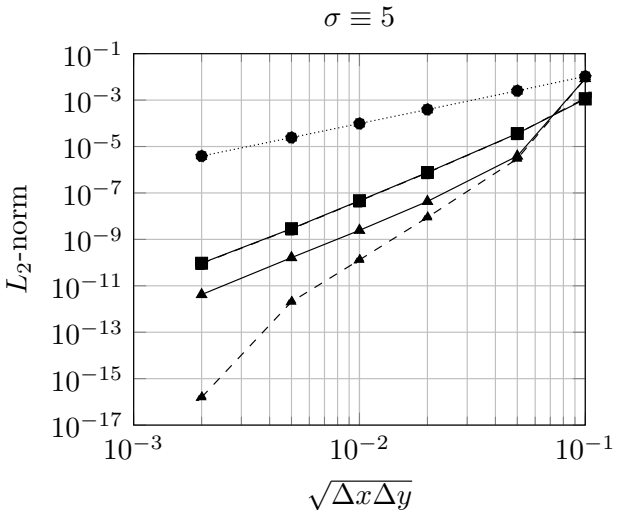

(a) Smooth gradient

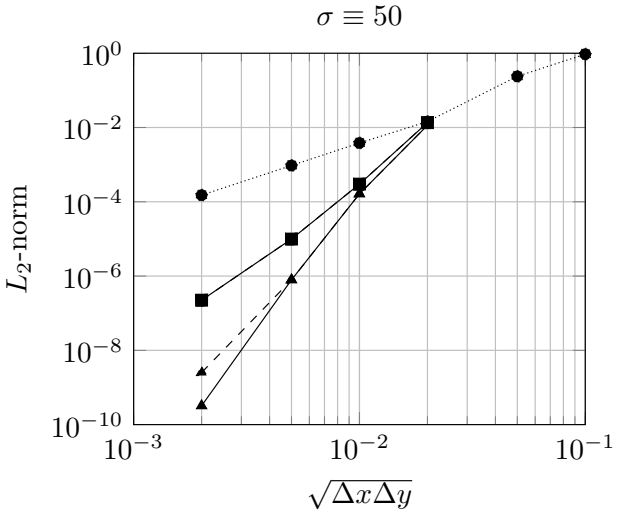

(b) Sharp gradient

Figure 15: Convergence plots for two values of σ: **Black Circle and densely dotted line**, FV-CF scheme; **Black Square and solid line**, 4th-order CIR + 4th-order CCS; **Black Square and dashed line**, 6th-order CIR + 4th-order CCS; **Black Triangle and solid line**, 4th-order CIR + 6th-order CCS; **Black Triangle and dashed line**, 6th-order CIR + 6th-order CCS.

not only the algorithm provides the value of the definite integral over the whole domain but also of each interval.

The Fourier analysis showed that when some values of α and β are employed, diffusive errors are not introduced for the integrals in the intervals. Each one of the rules developed in the previous section was compared in some numerical tests. They showed to work in a more than acceptable way with the exception of the 8th-order rule.

It would be interesting to use a non-uniform discretization [19] by rewriting all the derivations of CIR with a variable length h_i or apply a transformation $\xi = \xi(x)$ where the nodes are equidistant. More work is required to understand the abnormal behaviour of the eighth-order rule and to move to higher dimensions.

Conflict of interest

There is none.

Acknowledgements

The section of *CIR as a linear multistep* was prompted by the comment of one of the reviewers where he/she pointed out the analogy between CIR and a linear multistep method. The authors were unaware of this analogy and want to acknowledge his/her comment. In the course of this research the first author enjoyed a three-month stay in the CASA group of the University of Eindhoven, whose hospitality is recognized. The study was supported by the European Union through FEDER funding and Diputación General de Aragón "Construyendo Europa desde Aragón" [Government of Aragon "Building Europe from Aragon"], support that is gratefully acknowledged.

References

[1] Lele S.K., *Compact finite difference schemes with spectral-like resolution*, Journal of Computational Physics **103**, (1992) 16-42, doi:10.1016/0021-9991(92)90324-R

[2] Ahlberg J. H., Nilson E. N., *Convergence properties of the spline fit*, SIAM **11**, (1963) 95-104, doi:10.1137/0111007

[3] Qi L., *Some Simple Estimates for Singular Values of a Matrix*, Linear Algebra and its Applications **56**, (1984) 105-119, doi:10.1016/0024-3795(84)90117-4

[4] Anderson Jr. J.D., *Computational Fluid Dynamics. The Basics with Applications*, McGraw-Hill, (1995)

[5] Andersson B., Andersson R., Håkansson L., Mortensen M., Sudiyo R., van Wachem B., Hellström L., *Computational fluid dynamics for engineers*, Cambridge University Press, (2012)

[6] Wendt J.F., *Computational Fluid Dynamics. An Introduction*, Springer-Verlag Berlin Heidelberg, (2009)

[7] Pletcher R.H., Tannehill J.C., Anderson D.A., *Computational Fluid Mechanics and Heat Transfer*, CRC Press, (2013)

[8] Vichnevetsky R. and Bowles J.B., *Fourier Analysis of Numerical Approximations of Hyperbolic Equations*, SIAM Studies in Applied and Numerical Mathematics, (1989), doi:10.1137/1.9781611970876

[9] Sumi T. and Kurotaki T., *A new central compact finite difference formula for improving robustness in weighted compact nonlinear schemes*, Computers and Fluids **123**, (2015) 162-182, doi:10.1016/j.compfluid.2015.09.012

[10] Sen S., *Fourth order compact schemes for variable coefficient parabolic problems with mixed derivatives*, Computers and Fluids **134-135**, (2016) 81-89, doi:10.1016/j.compfluid.2016.05.002

[11] Lee S.T., Liu J., Sunc H.-W., *Combined compact difference scheme for linear second-order partial differential equations with mixed derivative*, Journal of Computational and Applied Mathematics **264**, (2014) 23-37, doi:10.1016/j.cam.2014.01.004

[12] Pascau A. and Arici M., *An accurate discretization for an inhomogeneous transport equation with arbitrary coefficients and source*, Computers and Fluids **125**, (2016) 101-115, doi:10.1016/j.compfluid.2015.11.006

[13] David B., *Integral Transforms and Their Applications*, Springer-Verlag New York, (2002)

[14] Pascau A., *An exact discretization for a transport equation with piecewise-constant coefficients and arbitrary source*, Computers and Fluids **75**, (2013) 42-50, doi:10.1016/j.compfluid.2013.01.009

[15] Wong H.H. and Raithby G.D., *Improved finite-difference methods based on a critical evaluation of the approximation errors*, Numerical Heat Transfer **2**, (1979) 139-163, doi:10.1080/10407787908913404

[16] Boersma B.J., *A staggered compact finite difference formulation for the compressible NavierStokes equations*, Journal of Computational Physics **208**, (2005)) 675690, doi:10.1016/j.jcp.2005.03.004

[17] ten Thije Boonkkamp J.H.M. and Anthonissen M.J.H., *The Finite Volume-Complete Flux Scheme for Advection-Diffusion-Reaction Equations*, Journal of Scientific Computing **46**, (2011) 47-70, doi:10.1007/s10915-010-9388-8

[18] van den Berkmortel S., Anthonissen M.J.H. and ten Thije Boonkkamp J.H.M., *Extension of the Finite Volume-Complete Flux scheme to linear source terms*, Student thesis: Bachelor, (2016), Link to the publication: research.tue.nl

[19] Gamet L., Ducros F., Nicoud F., Poinsot T., *Compact finite difference schemes on non-uniform meshes. Application to direct numerical simulations of compressible flows*, International Journal for Numerical Methods in Fluids **29**, (1999) 159191, doi: 10.1002/(SICI)1097-0363(19990130)29:2